Thermochemical and Kinetic Analysis of the Formyl Methyl Radical + O_2 Reaction System

Jongwoo Lee and Joseph W. Bozzelli*

Department of Chemical Engineering and Chemistry, New Jersey Institute of Technology, Newark, New Jersey 07102

Received: January 2, 2003; In Final Form: March 14, 2003

Thermochemical properties for important species in the formyl methyl radical ($C^{\bullet}H_2CHO$) + O_2 reaction system are analyzed to evaluate reaction paths and kinetics in both oxidation and pyrolysis. Enthalpies of formation ($\Delta H_f^\circ{}_{298}$) are determined using isodesmic reaction analysis at the CBSQ composite and density functional levels. Entropies ($S^\circ{}_{298}$) and heat capacities [$C_p^\circ(T)$] are determined using geometric parameters and vibrational frequencies obtained at the HF/6-31G(d′) level of theory. Internal rotor contributions are included in S and $C_p(T)$ values. The formyl methyl radical adds to O_2 to form a $C(OO^{\bullet})H_2CHO$ peroxy radical with a 27.5 kcal/mol well depth. The peroxy radical can undergo dissociation back to reactants, decompose to $CH_2CO + HO_2$ via HO_2 elimination, or isomerize via hydrogen shift to form a $C(OOH)H_2C^{\bullet}O$. This $C(OOH)H_2C^{\bullet}O$ isomer can undergo β scission to products, $CH_2CO + HO_2$, decompose to $CO + CH_2O + OH$, or decompose to a diradical, $CH_2O^{\bullet}C^{\bullet}O + OH$ via simple RO−OH bond cleavage. Rate constants are estimated as a function of pressure and temperature using quantum Rice−Ramsperger−Kassel (QRRK) analysis for $k(E)$ and master equation for falloff. Important reaction products are stabilization of the $C(OO^{\bullet})H_2CHO$ peroxy adduct at low temperature and $CO + CH_2O + OH$ products via intramolecular H shift at high temperature. $\Delta H_f^\circ{}_{298}$ values are estimated for the following compounds at the CBSQ level: $C^{\bullet}H_2CHO$ (3.52 kcal/mol), $C(OOH)H_2CHO$ (−56.19 kcal/mol), $C(OO^{\bullet})H_2CHO$ (−21.01 kcal/mol), $C(OOH)H_2C^{\bullet}O$ (−19.64 kcal/mol). A mechanism for pyrolysis and oxidation of the formyl methyl radical is constructed, and the reaction of the formyl methyl radical with O_2 versus unimolecular decomposition is evaluated.

1. Introduction

Acetaldehyde and the radical species that result through loss of hydrogen atoms from the carbon sites in CH_3CHO are common products (intermediates) from the oxidation of higher molecular weight hydrocarbon species in combustion and in atmospheric chemistry. Oxidation of methane also forms these species as a result of methyl radical combination and subsequent reactions of the ethane. The association reaction of these radicals with molecular oxygen ($^3O_2$) will form chemically activated peroxy adducts that can be stabilized, or the adduct may react via isomerization to new products before stabilization. The adducts can also dissociate back to initial reactants. These reactions are complex, because of competition between the pressure-dependent stabilization and unimolecular reaction to new products or reverse dissociation.[1,2] The isomerization, dissociation, and bimolecular reactions of the stabilized adduct provide further complexity. The reactions of radicals from acetaldehyde with oxygen also serve as model reactions for some reaction paths of larger aldehydic molecule systems. This study focuses on the reaction mechanism of the formyl methyl radical association with O_2.

Bozzelli et al.[3,4] and Mebel et al.[5] have separately reported that the formyl methyl radical is an important intermediate from the reaction of vinyl radicals, for example, the $C_2H_3 + O_2$ reaction system. The $C_2H_3O + O$ product set is important at low pressures, and it is important above 900 K at atmospheric pressure.

$$C_2H_3 + O_2 \rightarrow C_2H_3O \text{ (or } C^{\bullet}H_2CH{=}O) + O \qquad (1)$$

SCHEME 1: One Reaction Path for Propene + Ozone

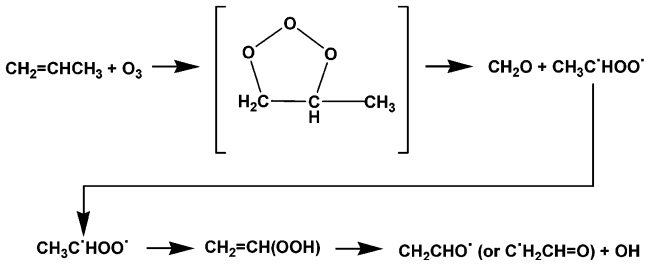

The $C^{\bullet}H_2CH{=}O$ radical is also formed in a number of peroxide reactions important in intermediate temperature combustion and thermal oxidation.[6,7]

Olzmann et al.[8] and Atkinson et al.[9,10] have shown that formyl methyl radicals are formed in ozone reactions of olefins, where the Criegee intermediate $CH_3C^{\bullet}HOO^{\bullet}$ undergoes an H shift to form a vinyl peroxide, which dissociates rapidly through cleavage of the weak CH_2CHO−OH bond. An example formation of $C^{\bullet}H_2CH{=}O$ in one reaction path for propene with ozone is illustrated in Scheme 1.

2. Previous Studies

Reactions involving abstraction of H atoms from acetaldehyde by Cl, F, and OH radicals have been studied by several research groups.[11−18] Although the abstraction can occur at two sites, these studies all report that the dominant reaction at atmospheric temperature is the abstraction from the carbonyl site to produce acetyl radicals. Sehested et al.[11] are one group that have reported data for the abstraction of hydrogen atoms, by atomic fluorine, on the methyl radicals. They reported formyl methyl radical production at 35% and acetyl at 65% (both ±9%) at 295 K and

* Author to whom correspondence should be addressed [e-mail Bozzelli@njit.edu; telephone (973) 596-5294; fax (973) 596-3586].

10.1021/jp030001o CCC: $25.00
Published on Web 04/12/2003

SCHEME 2: Enthalpies of Formation at CBS-Q, CBS-QCI/APNO, and G2 Methods with Experimental Values

Species	Enthalpies of Formation ($\Delta H_f^\circ{}_{298}$) in kcal/mol				
	CBS-Q	CBS-QCI/APNO	G2	Ref.	Exp. [ref]
$CH_3C\bullet(=O)$	-3.08 ± 0.38	-3.27 ± 0.28	-	29	-2.90 ± 0.70 [31]
$C\bullet H_2CHO$	3.52 ± 0.38	3.08 ± 0.28	-	29	3.55 ± 1.00 [32]
$CH_3OO\bullet$	0.3 ± 2.4	1.2 ± 1.7	-	30	2.15 ± 1.22 [33]
CH_3CH_2OOH	-39.9 ± 1.5	-	-40.1 ± 1.8	30	-39.7 ± 0.3[a] [34]
$CH_3CH_2OO\bullet$	-6.7 ± 2.3	-	-6.8 ± 2.7	30	-6.8 ± 2.3 [35]
$C\bullet H_2CH_2OOH$	11.2 ± 2.1	-	10.5 ± 2.4	30	10.96 ± 1.06[a] [34]

[a] Calculation values.

1000 mbar. Abstraction from the methyl group producing a formyl methyl radical should become important, at increased temperatures because of the higher degeneracy and reduced influence of the activation energy (E_a).

Alvarez-Idaboy et al.[17] have recently performed computational chemistry studies to characterize the abstraction reaction of OH + acetaldehyde at the CCSD(T)/6-311++G(d,p)//MP2(FC)/6-311++G(d,p) level of theory. These results also indicate that the reaction occurs predominantly by hydrogen abstraction from the carbonyl site; they reported that OH addition to the carbonyl carbon has a barrier of 9.31 kcal/mol and is unfavorable relative to the abstraction.

Formyl methyl was generated by photodissociation of methyl vinyl ether at 298 K by Zhu and Johnston;[19] $CH_3-O-C_2H_3 + h\upsilon \rightarrow CH_3 + C_2H_3O$. Here the vinoxy radical undergoes rapid electron rearrangement to the lower energy (~16 kcal/mol lower) formyl methyl structure. Kinetic studies on this formyl methyl radical with O_2 show a slower reaction, $k = 1.2 \times 10^{11}$ cm^3/(mol·s), relative to that reported[3] for the acetyl radical, $k = 2.65 \times 10^{12}$ cm^3/(mol·s). This suggests that formyl methyl radicals produced in experiments on Cl or OH reaction with acetaldehyde will react about $^1/_{10}$ as fast with O_2, probably requiring little or no correction to kinetic data of the faster acetyl + O_2 reactions. It also suggests that a barrier to the association may exist or that there is a very low well depth for the formyl methyl + O_2 adduct.

Thermochemical properties are estimated for reactants, intermediates, products, and transition states in the reaction paths using ab initio and density functional calculations. The thermochemical parameters are used to calculate high-pressure-limit rate constants using canonical transition state theory (TST). Rate constants as a function of temperature and pressure are estimated using a multifrequency quantum RRK analysis for $k(E)$ and master equation analysis for falloff. The thermochemical and kinetic data at relevant pressures and temperatures should be useful to both atmospheric and combustion models.

3. Calculation Method

Enthalpies of formation ($\Delta H_f^\circ{}_{298}$) for reactants, intermediate radicals, transition states, and products are calculated using the CBS-Q composite method and density functional [B3LYP/6-31G(d)] calculations. The initial structure of each compound or transition state is determined using ROHF or UHF/PM3 in MOPAC,[20] followed by optimization and vibrational frequency calculation at the HF/6-31G(d′) level of theory using Gaussian 94[21] for the CBS-Q analysis. The prime in 6-31G(d′) indicates the basis set orbitals of Petersson et al.[22,23] Transition state geometries are identified by the existence of only one imaginary frequency, structure information, and the TST reaction coordinate vibration information. Zero-point vibrational energies (ZPVE) are scaled by 0.91844 as recommended by Ochterski et al.[24] Single-point energy calculations are carried out at the B3LYP/6-31G(d) level.

SCHEME 3: CBS-Q Calculation Sequence

	Level of Theory
Optimized Geometry	MP2/6-31G(d')
Single Point Calculation	QCISD(T)/6-31+G(d')
	MP4(SDQ)/CBSB4[a]
	MP2/CBSB3[b] CBSExtrap = (Nmin[c]=10, Pop[d])

[a] 6-31+G(d(f),d,p). [b]H, He 311+G(2p), Li−Ne 6-311+G(2df). [c]Minimum number of natural orbital configurations used for CBS extrapolations. [d]Use population localization.

Ochterski et al.[24] have developed several high-level, complete basis set (CBS) composite methods, denoted CBS-QCI/APNO and CBS-Q. They indicate that CBS-Q is the most accurate for molecules with several heavy atoms, whereas CBS-QCI/APNO is more accurate but can be used only on smaller molecules. The mean absolute deviations from experiment for the 125 energies of the G2 test set are 0.5 and 1.0 kcal/mol for CBS-QCI/APNO and CBS-Q, respectively. Curtiss and co-workers[25] also have evaluated the CBS-Q method using isodesmic bond separation reactions, rather than atomization energies, on the G2 neutral test set of 148 molecules. The average absolute deviation between experiment and the CBS-Q calculated enthalpies was 1.57 kcal/mol. They reported that the combination of such bond balance reactions with G2 theory leads to a dramatic improvement in the accuracy of theoretically evaluated enthalpies of formation.[26] We note that similar isodesmic reactions are used in this study. We[27−30] have studied $\Delta H_f^\circ{}_{298}$ values of hydrocarbons, substituted hydrocarbons, and corresponding radicals and show[27,28] that the CBS-Q values are in agreement with accepted literature values. The CBS-Q enthalpies are more consistent than QCISD(T)/6-31G(d,p) single-point calculations when values of one species are compared through a series of different work reactions. A comparison of ($\Delta H_f^\circ{}_{298}$) values from CBS-Q, CBS-QCI/APNO, and G2 methods with experimental values on several oxygenated hydrocarbons is given in Scheme 2.

The CBS-Q calculation sequence has the following steps at the noted levels (Scheme 3). It also includes a correction for spin contamination and an empirical correction (for the absolute overlap integral and the intraorbital interference factor). The CBS-Q calculation is indicated as being equivalent to a QCISD-(T)/6-311+G(3df,2p) calculation.[36,37] The complete basis set

(CBS-Q) method of Petersson and co-workers for computing accurate energies[23,24,38] is chosen as the determining enthalpies used in our kinetic analysis.

3.1. Determination of Enthalpies of Formation. The method of isodesmic reactions is used to determine the enthalpy of formation ($\Delta H_f^\circ{}_{298}$) for parent and radical species. It provides higher accuracy for estimates of $\Delta H_f^\circ{}_{298}$ than heats of atomization.[39−43]

The working reactions for estimation of $\Delta H_f^\circ{}_{298}$ on $CH_3C\bullet O$ are

$$CH_3C^\bullet O + CH_3CH_3 \leftrightarrow CH_3CHO + CH_3C^\bullet H_2 \quad \text{(IR1)}$$

$$CH_3C^\bullet O + CH_3OH \leftrightarrow CH_3CHO + C^\bullet H_2OH \quad \text{(IR2)}$$

$$CH_3C^\bullet O + CH_3C(=O)CH_3 \leftrightarrow CH_3CHO + C^\bullet H_2C(=O)CH_3 \quad \text{(IR3)}$$

The working reactions for estimation of $\Delta H_f^\circ{}_{298}$ on $C^\bullet H_2$-CHO are

$$C^\bullet H_2CHO + CH_3CH_3 \leftrightarrow CH_3CHO + CH_3C^\bullet H_2 \quad \text{(IR4)}$$

$$C^\bullet H_2CHO + CH_3OH \leftrightarrow CH_3CHO + C^\bullet H_2OH \quad \text{(IR5)}$$

$$C^\bullet H_2CHO + CH_3C(=O)CH_3 \leftrightarrow CH_3CHO + C^\bullet H_2C(=O)CH_3 \quad \text{(IR6)}$$

$\Delta H_f^\circ{}_{298}$ for the estimation of $C(OOH)H_2CHO$ is by

$$C(OOH)H_2CHO + CH_3CH_3 \leftrightarrow CH_3CHO + CH_3CH_2OOH \quad \text{(IR7)}$$

$\Delta H_f^\circ{}_{298}$ for the estimation of $C(OOH)H_2C^\bullet O$ ($^\bullet$ = radical site) is by

$$C(OOH)H_2C^\bullet O + CH_3CH_3 \leftrightarrow C(OOH)H_2CHO + CH_3C^\bullet H_2 \quad \text{(IR8)}$$

$$C(OOH)H_2C^\bullet O + CH_3CHO \leftrightarrow C(OOH)H_2CHO + CH_3C^\bullet O \quad \text{(IR9)}$$

$\Delta H_f^\circ{}_{298}$ for the estimation of $C(OO^\bullet)H_2CHO$ is by

$$C(OO^\bullet)H_2CHO + CH_3OOH \leftrightarrow C(OOH)H_2CHO + CH_3OO^\bullet \quad \text{(IR10)}$$

$$C(OO^\bullet)H_2CHO + CH_3CH_3OOH \leftrightarrow C(OOH)H_2CHO + CH_3CH_3OO^\bullet \quad \text{(IR11)}$$

Ab initio calculations for ZPVE and thermal correction energy are performed on all four compounds in the reaction. The three reference compounds in the working reaction (IR1), except the target molecule, $CH_3C^\bullet O$ in (IR1), have experimentally or theoretically determined values of $\Delta H_f^\circ{}_{298}$. The unknown $\Delta H_f^\circ{}_{298}$ of $CH_3C^\bullet O$ is obtained with the calculated $\Delta H^\circ{}_{rxn(298)}$ and the known $\Delta H_f^\circ{}_{298}$ of the three reference compounds. The $C^\bullet H_2CHO$, $C(OOH)H_2CHO$, $C(OOH)H_2C^\bullet O$, and $C(OO^\bullet)H_2$-CHO are calculated in the same manner.

Enthalpies of Transition States. $\Delta H_f^\circ{}_{298}$ values of transition state structures are estimated by evaluation of $\Delta H_f^\circ{}_{298}$ of the stable radical adducts from the working reaction analysis above, plus the difference of total energies between these radical species and the transition state. The method is illustrated for the H-shift transition state T_1HS in Scheme 4.

SCHEME 4: $\Delta H_f^\circ{}_{TS}$ (T_1HS) Calculation

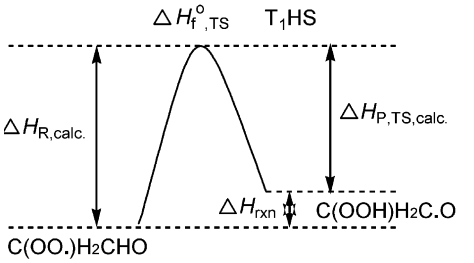

$$\Delta H_{R',TS,calc.} = \Delta H_{rxn}\ (\text{Reactant -> TS}) - \Delta H_{rxn}$$

$$\Delta H_{P,TS,calc.} = \Delta H_{rxn}\ (\text{Product -> TS})$$

$$\Delta H_f^\circ{}_{TS} = (\Delta H_{R',TS,calc.} + \Delta H_{P,TS,calc.}) / 2$$

Calculation of the enthalpy of formation for T_1HS is not taken as the calculated energy difference between reactant and transition state. The absolute enthalpies of reactant and product are first estimated using isodesmic reaction analysis (eqs IR8−IR11), and ΔH_{rxn} is taken from ΔH_f° values determined from the separate isodesmic reactions. $\Delta H_f^\circ{}_{TS}$ then is calculated by an average of two values $\Delta H_{R',TS,calcd}$ and $\Delta H_{P,TS,calcd}$. $\Delta H_{R',TS,calcd}$ is the difference between the calculated energy of the transition state and reactant minus ΔH_{rxn} ($\Delta H_f^\circ{}_{product} - \Delta H_f^\circ{}_{reactant}$). $\Delta H_{P,TS,calcd}$ is the difference between the calculated energy of the transition state and product.

3.2. Determination of Entropy and Heat Capacity. The contributions of vibrations and external rotation to entropies and heat capacities are calculated from scaled vibration frequencies and moments of inertia for the optimized HF/6-31G(d′) structures. Contributions to S and $C_p(T)$ from torsion frequencies corresponding to hindered internal rotation are replaced with values calculated from the method of Pitzer and Gwinn.[44] The number of optical isomers and spin degeneracy of unpaired electrons are also incorporated.

3.3. High-Pressure-Limit *A* Factors (*A*) and Rate Constant (k_∞) Determination. For the reactions where thermochemical properties of transition states are calculated by ab initio or density functional methods, k_∞ values are fit by three parameters, A, n, and E_a, over the temperature range from 298 to 2000 K, $k_\infty = A(T)^n \exp(-E_a/RT)$. Entropy differences between reactant and transition state are used to determine the pre-exponential factor, A, via canonical TST

$$A = (k_bT/h_p)\exp(\Delta S^\ddagger/R) \qquad E_a = \Delta H^\ddagger$$

where h_p is the Planck constant and k_b is the Boltzmann constant. Treatment of the internal rotors for S and $C_p(T)$ is important here because these internal rotors are often lost in the cyclic transition state structures.

Tunneling. Corrections for H-atom tunneling are applied for the intramolecular hydrogen atom transfer reactions of T_1HS and $TC^\bullet CHOS$ and hydrogen atom dissociation reactions $TC^\bullet CHO-H$ and $TCC^\bullet O-H$. The tunneling corrections are determined using the Erwin−Henry computer code[45] that is based on Eckart's one-dimensional potential function.[46] The Erwin−Henry code requires input of vibrational frequencies, moments of inertia, symmetries, electronic degeneracies, and total energies at 0 K of reactants, transition states, and products; imaginary frequencies are also required. Schwartz et al.[47] note

TABLE 1: Enthalpies of Formation for Reference Molecules in the Isodesmic Reactions

compound	$\Delta H_f^\circ{}_{298}$ (kcal/mol) [ref]	compound	$\Delta H_f^\circ{}_{298}$ (kcal/mol) [ref]
C_2H_6	-20.24 ± 0.10^a [52]	CH_3CHO	-39.72 ± 0.12^a [53]
C_2H_5OOH	-39.70 ± 0.3 [34]	$CH_3C^\bullet H_2$	28.80 ± 0.50 [54]
CH_3OOH	-31.80 [40]	$CH_3OO^\bullet$	2.15 ± 1.22 [33]
CH_3OH	-48.16 ± 0.07 [55]	$C^\bullet H_2OH$	-3.97 ± 0.22 [56]
$CH_3C(=O)CH_3$	-51.94 ± 0.17 [55]	$C^\bullet H_2C(=O)CH_3$	-8.53 ± 1.15 [43]
$C_2H_5OO^\bullet$	-6.72 ± 2.3 [30]	C_2H_5OH	-56.17 ± 0.10^a [53]
$CH_3C(=O)OH$	-103.56 ± 0.32^b	$C_2H_5O^\bullet$	-3.90 ± 1.27 [42]

[a] Uncertainties are evaluated from ref 55. [b] Average of -103.32 (ref 53), -103.44 (ref 55), and -103.92 (ref 57).

TABLE 2: Reaction Enthalpies and Enthalpies of Formation in the Isodesmic Reactions

	$\Delta H^\circ_{rxn,298}$ (kcal/mol)		$\Delta H_f^\circ{}_{298}$ (kcal/mol)	
working reaction series	B3LYP	CBSQ	B3LYP	CBSQ
$CH_3C^\bullet O + CH_3CH_3 \leftrightarrow CH_3CHO + CH_3C^\bullet H_2$		12.26		-2.94
$CH_3C^\bullet O + CH_3OH \leftrightarrow CH_3CHO + C^\bullet H_2OH$		7.25		-2.78
$CH_3C^\bullet O + CH_3C(=O)CH_3 \leftrightarrow CH_3CHO + C^\bullet H_2C(=O)CH_3$		7.20		-3.51
av for $CH_3C^\bullet O$:				-3.08 ± 0.38 (CBSQ)
$C^\bullet H_2CHO + CH_3CH_3 \leftrightarrow CH_3CHO + CH_3C^\bullet H_2$		5.66		3.66
$C^\bullet H_2CHO + CH_3OH \leftrightarrow CH_3CHO + C^\bullet H_2OH$		0.65		3.82
$C^\bullet H_2CHO + CH_3C(=O)CH_3 \leftrightarrow CH_3CHO + C^\bullet H_2C(=O)CH_3$		0.60		3.09
av for $C^\bullet H_2CHO$:				3.52 ± 0.38 (CBSQ)
$C(OOH)H_2CHO + C_2H_6 \leftrightarrow CH_3CHO + C_2H_5OOH$	-3.16	-2.99	-56.02	-56.19
$C(OOH)H_2C^\bullet O + C_2H_6 \leftrightarrow C(OOH)H_2CHO + CH_3C^\bullet H_2$	13.29	12.46	-20.27	-19.61
$C(OOH)H_2C^\bullet O + CH_3CHO \leftrightarrow C(OOH)H_2CHO + CH_3C^\bullet O$	1.01	0.12	-20.39	-19.67
				-20.33 ± 0.09 (B3LYP)
av for $C(OOH)H_2C^\bullet O$:				-19.64 ± 0.04 (CBSQ)
$C(OO^\bullet)H_2CHO + CH_3OOH \leftrightarrow C(OOH)H_2CHO + CH_3OO^\bullet$	-1.14	-1.40	-20.93	-20.84
$C(OO^\bullet)H_2CHO + C_2H_5OOH \leftrightarrow C(OOH)H_2CHO + C_2H_5OO^\bullet$	-1.45	-2.03	-21.59	-21.18
				-21.26 ± 0.47 (B3LYP)
av for $C(OO^\bullet)H_2CHO$:				-21.01 ± 0.24 (CBSQ)

that calculated vibrational frequencies using the HF/6-31G(d) level of theory need to be reduced by half to one-third for calculated transition states rate constant to match experimental data in abstraction reactions from fluorinated methanes.

3.4. Kinetic Analysis. Thermochemical properties for each species on the potential energy surface for the reaction system are evaluated. Forward or reverse rate constants (high-pressure limit) for each elementary reaction step are determined from the calculations and use of literature data for enthalpies of stable molecules. Reverse rate constants are calculated from microscopic reversibility.

Multifrequency quantum Rice−Ramsperger−Kassel (QRRK) analysis is used to calculate $k(E)$ with a master equation analysis[30] for falloff in order to obtain rate constants as a function of temperature and pressure. This kinetic analysis is for the chemical activation and the dissociation reaction systems. The master equation analysis[30] uses an exponential-down model for the energy transfer function with $(\Delta E)^\circ_{down} = 1000$ cal/mol[48,49] for N_2 as the third body and a 500 cal energy gain is used.

The QRRK/master equation analysis is described by Chang et al.[4,30] The QRRK code utilizes a reduced set of three vibration frequencies that accurately reproduce the molecules' heat capacities; the code includes contribution from one external rotation in the calculation of the ratio of the density of states to the partition coefficient $\rho(E)/Q$.

Comparisons of ratios of these $\rho(E)/Q$ with direct count $\rho(E)/Q$ values have been shown to result in good agreement.[50] Rate constant results from the QRRK−Master equation analysis are shown to accurately reproduce (model) experimental data on several complex systems.[4,30,51] They also provide a reasonable method to estimate rate constants for numerical integration codes by which the effects of temperature and pressure can be incorporated in these chemical activation systems.

4. Results and Discussion

4.1. Geometries of Parent Hydroperoxide Aldehyde, Two Intermediate Radicals, and Transition States. Tables IS [a] to IS [c] (Supporting Information) show the MP2/6-31G(d′) optimized geometries of the $C(OOH)H_2CHO$ and the two intermediate radicals, $C(OO^\bullet)H_2CHO$ and $C(OOH)H_2C^\bullet O$, respectively. All remaining structures are from MP2/6-31G(d′)-determined geometries except transition states: $T_1E(HO_2)$, $T_2E(C^\bullet H_2OOH)$, and $T_2D(CO + CH_2O + OH)$, which are determined from B3LYP/6-31G(d) calculations. Energies of activation (E_a) reported below are relative to the corresponding stabilized adduct.

$TC^\bullet H_2CHO-O_2$ is the transition state (TS) structure for $C^\bullet H_2CHO$ addition to O_2 to form the $C(OO^\bullet)H_2CHO$ peroxy radical. There is a small barrier to reaction, 2.97 kcal/mol, and the well depth is 27.5 kcal/mol. The $C^\bullet H_2CHO$ structure is planar with the O_2 group perpendicular to the plane and the forming O_7-C_1 bond is calculated as 1.91 Å.

$T_1E(HO_2)$ shows the B3LYP/6-31G(d) geometry of the TS structure for direct HO_2 elimination from the peroxy adduct: $C(OO^\bullet)H_2CHO$ to $CH_2CO + HO_2$. The O_7-O_8 bond shortens from 1.32 to 1.26 Å, whereas the O_7-C_1 and H_6-C_2 cleaving bonds lengthen to 2.31 and 1.31 Å, respectively. The E_a is 48.13 kcal/mol.

The H-shift isomerization $C(OO^\bullet)H_2CHO \rightarrow C(OOH)H_2C^\bullet O$ is T_1HS. The H_4 atom is in a bridge structure shifting from C_2 to the radical site O_5. The leaving H_4-C_2 bond is 1.29 Å, and the forming H_4-O_5 bond is 1.36 Å. The imaginary frequency is 3104 cm^{-1} at HF/6-31G(d′), and the E_a is 20.25 kcal/mol. The $C(OOH)H_2C^\bullet O$ isomer is only slightly, 1.4 kcal/mol, higher in energy than the peroxy isomer.

The TS structure for HO_2 elimination from the hydroperoxide acetyl radical adduct is $T_2E(HO_2)$: $C(OOH)H_2C^\bullet O \rightarrow CH_2CO + HO_2$. The cleaving O_6-C_1 bond is 1.86 Å, and the C_1-C_4

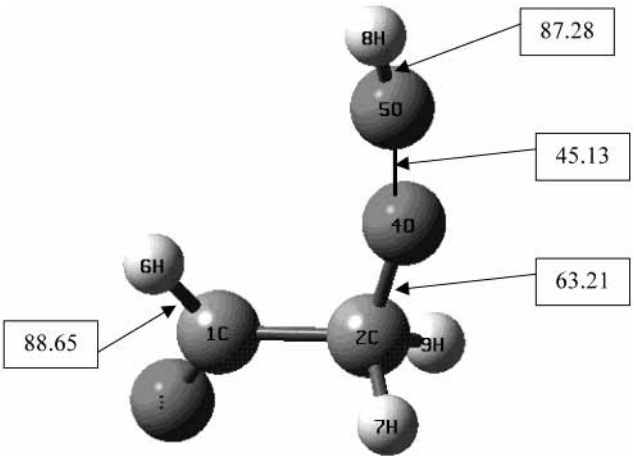

Figure 1. Bond dissociation energy (kcal/mol) of $C(OOH)H_2CHO$.

TABLE 3: Comparison of Bond Energies (Kilocalories per Mole) between $C(OOH)H_2C(=O)H$, C_2H_5OOH, and $CH_3C(=O)OOH$

	$C(OOH)H_2CHO$[a]	C_2H_5OOH[b]	$CH_3C(=O)OOH$[c]
ROO- -H	87.28	85.27	98.33
RO- -OH	45.13	45.12	50.95
R- -OOH	63.21	71.35	85.22
$C(OOH)H_2C(=O)$- -H	88.65		
H- $-CH_2CH_2OOH$		103.21	
H- $-CH_2C(=O)OOH$			103.95
CH_3CH_2O- -H		104.7 ± 0.8[d]	
$CH_3C(=O)O$- -H			112.32[e]

[a] In this study. [b] Reference 30. [c] Reference 58. [d] Reference 59. [e] $\Delta H_f°_{298}$ of $CH_3C(=O)OH = -103.56$ (average of refs 53, 55, and 57), $CH_3C(=O)O^{\bullet} = -43.34$ (CBSQ with isodesmic reaction, $CH_3C(=O)O^{\bullet} + C_2H_5OH \leftrightarrow CH_3C(=O)OH + C_2H_5O^{\bullet}$).

bond shortens from 1.54 to 1.35 Å. The CH_2CO is planar with the HO_2 group perpendicular to the plane.

The TS structure for β scission of $C(OOH)H_2C^{\bullet}O$ to products, $CO + C^{\bullet}H_2OOH$, is $T_2E(C^{\bullet}H_2OOH)$. The cleaving C_1-C_2 bond is 2.32 Å, and the transition state C_2-O_3 is moving to a double bond at 1.36 Å. The E_a is 10.32 kcal/mol. The TS structure for $C(OOH)H_2C^{\bullet}O$ decomposition to products, $CO + CH_2O + OH$, is $T_2D(CO + CH_2O + OH)$. The leaving C_2-C_3 and O_7-O_4 bonds are 1.69 and 1.81 Å, respectively. The E_a is 16.80 kcal/mol.

The TS structure for hydrogen abstraction from the $-CHO$ group of $C^{\bullet}H_2CHO$ by O_2 to form ketene plus HO_2 (bimolecular reaction), $C^{\bullet}H_2CHO + O_2 \rightarrow CH_2CO + HO_2$, is $TC^{\bullet}H_2CO-HO_2$. The H_6 atom is in a bridge structure shifting from C_2 to O_7. The transition state C_1-C_2 bond is 1.42 Å, and the leaving H_6-C_2 and the forming H_6-O_7 bonds are 1.35 and 1.28 Å, respectively. The imaginary frequency is 3425 cm^{-1} at HF/6-31G(d′), and the E_a is 29.03 kcal/mol.

$TCC^{\bullet}O-H$ is the transition state for $CH_3C^{\bullet}O$ reaction to $CH_2CO + H$. The C_1-C_4 bond is 1.34 Å, and the cleaving C_1-H_5 bond is 1.70 Å. The CH_2CO is planar with the hydrogen perpendicular to the plane.

The TS structure for β scission of $C^{\bullet}H_2CHO$ to $CH_2CO + H$ is $TC^{\bullet}CHO-H$. The cleaving C_4-H_5 bond is 1.64 Å. The CH_2CO is planar with the hydrogen perpendicular to the plane. The E_a is 40.49 kcal/mol.

The H-shift isomerization in the formyl methyl radical, $C^{\bullet}H_2CHO \rightarrow CH_3C^{\bullet}O$, is identified as $TC^{\bullet}CHOS$ in Supporting Information Table IS [m]. The H_4 atom is in a bridge structure shifting from C_2 to the radical site on C_1. The imaginary frequency is 2401 cm^{-1} at HF/6-31G(d′), and the E_a is 39.51 kcal/mol.

Table IS [n] shows the TS structure for unimolecular decomposition of the acetyl radical, $CH_3C^{\bullet}O \rightarrow CH_3 + CO$, TCH_3-CO. The leaving C_1-C_2 and the forming CO bond lengths are 2.11 and 1.16 Å, respectively. The E_a and $\Delta H_f°_{rxn,298}$ are 16.64 and 10.73 kcal/mol, respectively.

4.2. Enthalpy of Formation ($\Delta H_f°_{298}$) Using Calculated Total Energies and Isodesmic Reactions. The total energies at 0 K including scaled ZPVEs, thermal corrections to 298.15 K, and total energies at 298 K are listed in Table II

S for the CBSQ calculations. Frequencies are scaled by 0.91844 for HF/6-31G(d′)-determined frequencies as recommended by Ochterski et al.[24]

The evaluated enthalpies of formation for the reference molecules and radicals in the isodesmic reactions are listed in Table 1. The evaluated reaction enthalpies and enthalpies of formation in the isodesmic reactions are listed in Table 2.

The working reactions IR1−IR3 and IR4−IR6 are used to estimate enthalpies of $CH_3C^{\bullet}O$ and $C^{\bullet}H_2CHO$ radical species with the CBSQ composite method.

The average values of $\Delta H_f°_{298}$ from three isodesmic reactions for $CH_3C^{\bullet}O$ and $C^{\bullet}H_2CHO$ are −3.08 and 3.52 kcal/mol by CBSQ, respectively.

A low or zero $\Delta H°_{rxn,298}$ in working reactions where the central atom environments are similar on both sides suggests good cancellation of errors due to similarity in the reaction environment. This should lead to accurate $\Delta H_f°_{298}$ values. This also supports the hypothesis of group additivity. As an example, $\Delta H_f°_{298}[C(OOH)H_2CHO]$ is evaluated from

$$\Delta H_f°_{rxn,298} = \Delta H_f°_{298}[CH_3CHO] + \Delta H_f°_{298}[C_2H_5OOH] - \Delta H_f°_{298}[C(OOH)H_2CHO] - \Delta H_f°_{298}[C_2H_6]$$

$$\Delta H_f°_{rxn,298} = -2.99 \text{ (CBSQ) and } -3.16 \text{ (B3LYP)}$$

The enthalpies of formation for $C(OOH)H_2CHO$ are −56.19 and −56.02 kcal/mol by CBSQ and B3LYP/6-31G(d), respectively. The enthalpy of formation for the parent hydroperoxide is important because it allows the evaluation of relative stabilities in the peroxy radicals.

The bond energies of $C(OOH)H_2CHO$ (Figure 1), C_2H_5OOH, and $CH_3C(=O)OOH$ are compared in Table 3. The R−OOH

TABLE 4: Activation Energies and Enthalpies of Transition States in CBSQ Calculation (kcal/mol)

reactant	transition state (TS)	product	E_a	$\Delta H_f°_{298}$ of TS (kcal/mol)
$C(OO^{\bullet})H_2CHO$	T_1HS	$C(OOH)H_2C^{\bullet}O$	20.25	−0.76
$C(OO^{\bullet})H_2CHO$	$T_1E(HO_2)$[a,b]		48.31	27.30
$C(OOH)H_2C^{\bullet}O$	$T_2E(HO_2)$[a]		23.53	3.89
$C(OOH)H_2C^{\bullet}O$	$T_2E(C^{\bullet}H_2OOH)$[a,b]		10.32	−9.32
$C(OOH)H_2C^{\bullet}O$	$T_2D(CO + CH_2O + OH)$[a,b]		16.80	−2.84
$C^{\bullet}H_2CHO + O_2$	$TC^{\bullet}H_2CO-HO_2$	$CH_2CO + HO_2$	28.84	32.36

[a] The activation energy and enthalpy for this transition state are estimated by taking the difference of total energy with ZPVE and thermal correction between the transition state and reactant (peroxy/hydroperoxide isomer). [b] CBS-Q//B3LYP/6-31G(d) calculation.

TABLE 5: Ideal Gas Phase Thermodynamic Properties Obtained by CBSQ Calculation and by THERM[a]

species (s, e, OI)[b]		$\Delta H_f°_{298}$[c]	$S°_{298}$[d]	$C_{p,300}$[d]	$C_{p,400}$	$C_{p,500}$	$C_{p,600}$	$C_{p,800}$	$C_{p,1000}$	$C_{p,1500}$
CH_3CHO	TVR[e]		57.97[b]	11.58	14.29	16.88	19.20	22.98	25.80	30.10
(3,0,1)	internal rotor 1[f]		5.16	1.44	1.30	1.23	1.17	1.10	1.07	1.03
	total	−39.72	63.13	13.02	15.59	18.11	20.37	24.08	26.87	31.13
	THERM	−39.18	63.13	13.22	15.71	18.22	20.47	24.22	26.97	
$CH_3C^{\bullet}O$	TVR		58.82	11.12	13.24	15.24	17.01	19.90	22.07	25.39
(3,1/2,1)	internal rotor 1		5.45	1.16	1.10	1.06	1.04	1.02	1.01	1.00
	total	−3.08	64.27	12.28	14.34	16.30	18.05	20.92	23.08	26.39
	THERM	−2.54	64.27	12.28	14.34	16.30	18.05	20.92	23.08	
$C^{\bullet}H_2CHO$	TVR		61.99	13.10	15.79	18.04	19.86	22.63	24.62	27.66
(1,1/2,1)	total	3.52	61.99	13.10	15.79	18.04	19.86	22.63	24.62	27.66
	THERM	4.06	61.99	13.10	15.79	18.04	19.86	22.63	24.62	
$C(OOH)H_2CHO$	TVR		69.25	15.10	18.82	22.20	25.05	29.44	32.58	37.30
(1,0,2)	internal rotor 1, 2, 3		13.56	3.99	5.82	5.92	5.93	5.84	5.68	5.20
	total	−56.19	82.81	19.09	24.64	28.12	30.98	35.28	38.26	42.50
	THERM	−55.77	82.81	19.09	24.64	28.12	30.98	35.28	38.26	42.50
$C(OO^{\bullet})H_2CHO$	TVR		68.78	14.86	18.37	21.49	24.10	28.05	30.81	34.77
(1,1/2,1)	internal rotor 1, 2		11.20	2.27	4.13	3.98	3.84	3.68	3.62	3.48
	total	−21.01	79.98	17.13	22.50	25.47	27.94	31.73	34.43	38.25
	THERM	−20.17	79.98	17.13	22.50	25.47	27.94	31.73	34.43	38.25
$C(OOH)H_2C^{\bullet}O$	TVR		70.40	14.64	17.81	20.58	22.89	26.39	28.88	32.62
(1,1/2,2)	internal rotor 1, 2, 3		11.38	5.90	6.35	6.49	6.45	6.09	5.59	4.59
	total	−19.64	81.78	20.54	24.16	27.07	29.34	32.48	34.47	37.21
	THERM	−18.73	81.78	20.54	24.16	27.07	29.34	32.48	34.47	
$C^{\bullet}H_2OOH$	TVR		61.46	11.15	13.22	15.05	16.57	18.93	20.68	23.52
(1,1/2,2)	internal rotor 1, 2		4.77	3.61	4.05	4.33	4.48	4.45	4.19	3.44
	total		66.23	14.76	17.27	19.38	21.05	23.38	24.87	26.96
	THERM	15.20	65.41	15.60	18.12	20.15	21.79	24.14	25.65	27.65
$CH_2O^{\bullet}C^{\bullet}O$	TVR		66.26	13.36	15.79	17.84	19.53	22.10	23.91	26.53
(1,1,1)	internal rotor 1		5.91	2.19	1.95	1.74	1.58	1.37	1.25	1.12
	total	11.01	72.17	15.55	17.74	19.58	21.11	23.47	25.16	27.65
$HC^{\bullet}{=}C{=}O$	TVR		59.79	12.48	13.44	14.23	14.90	15.98	16.79	18.06
(1,1/2,1)	total	41.98	59.79	12.48	13.44	14.23	14.90	15.98	16.79	18.06
T_1HS	TVR		70.09	17.85	21.71	24.96	27.58	31.41	33.98	37.51
(1,1/2,2)	total	−0.76	70.09	17.85	21.71	24.96	27.58	31.41	33.98	37.51
$T_1E(HO_2)$	TVR		81.23	22.66	25.70	28.18	30.17	33.12	35.15	38.05
(1,1/2,2)	total	27.30	81.23	22.66	25.70	28.18	30.17	33.12	35.15	38.05
$T_2E(HO_2)$	TVR		70.81	16.98	19.98	22.41	24.37	27.35	29.52	32.89
(1,1/2,2)	internal rotor 1, 2		5.34	3.60	4.06	4.33	4.46	4.37	4.07	3.33
	total	3.89	76.15	20.58	24.04	26.74	28.83	31.72	33.59	36.22
$T_2E(C^{\bullet}H_2OOH)$	TVR		85.82	20.33	22.39	24.17	25.69	28.12	30.01	33.10
(1,1/2,2)	internal rotor 1, 2, 3		11.38	5.90	6.35	6.49	6.45	6.09	5.59	4.59
	total	−9.32	97.20	26.23	28.74	30.66	32.14	34.21	35.60	37.69
$T_2D(CO + CH_2O + OH)$	TVR		77.30	19.77	22.25	24.44	26.29	29.20	31.36	34.77
(1,1/2,1)	internal rotor 1		2.16	1.98	2.13	2.23	2.29	2.28	2.14	1.75
	total	−2.84	79.46	21.75	24.38	26.67	28.58	31.48	33.50	36.52
$TC^{\bullet}H_2CHO{-}O_2$	TVR		70.53	15.82	19.16	21.97	24.22	27.55	29.88	33.29
(1,1/2,1)	internal rotor 1, 2		11.20	2.27	4.13	3.98	3.84	3.68	3.62	3.48
	total	6.49	81.73	18.09	23.29	25.95	28.06	31.23	33.50	36.77
$TC^{\bullet}CHOS$	TVR		61.32	12.12	14.47	16.59	18.40	21.21	23.21	26.11
(1,1/2,1)	total	43.03	61.32	12.12	14.47	16.59	18.40	21.21	23.21	26.11
$TC^{\bullet}CHO{-}H$	TVR		64.09	15.29	17.59	19.33	20.71	22.79	24.31	26.64
(1,1/2,1)	total	44.01	64.09	15.29	17.59	19.33	20.71	22.79	24.31	26.64
TCC.O−H	TVR		63.25	14.69	17.05	18.88	20.34	22.53	24.12	26.54
(1,1/2,1)	total	40.09	63.25	14.69	17.05	18.88	20.34	22.53	24.12	26.54
$TCH_3{-}CO$	TVR		60.70	12.22	13.92	15.42	16.75	18.99	20.78	23.69
(3,1/2,1)	internal rotor 1		5.45	1.16	1.10	1.06	1.04	1.02	1.01	1.00
	total	13.56	66.15	13.38	15.02	16.48	17.79	20.01	21.79	24.69
$TC^{\bullet}H_2CHO{-}HO_2$	TVR		71.57	17.14	20.32	22.96	25.10	28.28	30.46	33.62
(1,1/2,1)	internal rotor 1, 2		6.31	4.15	4.41	4.44	4.34	3.96	3.57	2.91
	total	32.36	77.88	21.29	24.73	27.40	29.44	32.24	34.03	36.53

[a] Thermodynamic properties are referred to a standard state of an ideal gas of pure enantiometer at 1 atm. Therm values for stable species are included for comparison (refs 60 and 61). [b] Symmetry number, optical isomer and electronic spin are taken into account, −Rln(s), Rln2, and Rln2, respectively. s = number of symmetry, e = electronic spin, OI = number of optical isomer. [c] Units in kcal/mol. [d] Units in cal/mol·K. [e] Sum of contributions from translations, vibrations, and external rotations. [f] Contribution from internal rotation.

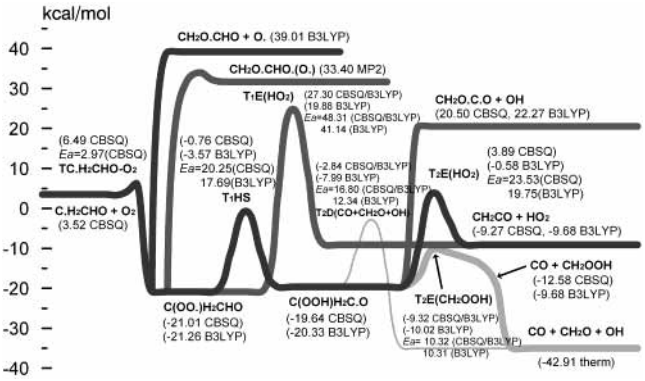

Figure 2. Potential energy diagram $C^{\bullet}H_2CHO + O_2$.

bond energy in $C(OOH)H_2CHO$ is 8 kcal/mol lower than that of C_2H_5OOH, because the radical site is resonantly stabilized. The RO−OH and ROO−H bonds in $C(OOH)H_2CHO$ are 45.1 and 87.3 kcal/mol, similar to those in C_2H_5OOH, 45.1 and 85.3 kcal/mol, respectively. However, the C−O, O−O, and O−H bond energies in $CH_3C(=O)OOH$ are 22, 6, and 11 kcal/mol higher than those in $C(OOH)H_2CHO$, respectively, because of coupling with the C=O carbonyl bond.

The enthalpies of formation of the two intermediate radicals, $C(OOH)H_2C^{\bullet}O$ and $C(OO^{\bullet})H_2CHO$, by CBSQ and B3LYP/6-31G(d) are obtained from the use of isodesmic reactions IR8−IR11 and values of reference species in Table 1. The data result in enthalpy values of −19.64 and −20.33 for $C(OOH)H_2C^{\bullet}O$ and −21.01 and −21.26 for $C(OO^{\bullet})H_2CHO$ by CBSQ and B3LYP/6-31G(d), respectively. The similar $\Delta H_f^{\circ}{}_{298}$ values for these two radicals imply nearly identical bond energies at the respective radical sites (within 1.4 kcal/mol and a thermoneutral reaction for the H shift).

The activation energies and enthalpies of transition states at CBS-Q level are summarized in Table 4. (E_a values are discussed in section 4.4.) All E_a values are at the CBS-Q level except the transition states: $T_1E(HO_2)$, $T_2E(C^{\bullet}H_2OOH)$, and $T_2D(CO + CH_2O + OH)$, which are determined from CBS-Q//B3LYP/6-31G(d) calculations because all attempts at MP2 optimization failed.

4.3. Entropy (S°_{298}) and Heat Capacity [$C_p(T)$, 300 ≤ T/K ≤ 1500]. S°_{298} and $C_p(T)$ values are calculated on the basis of vibration frequencies and moments of inertia from the optimized HF/6-31G(d′) structures (Tables IIIS and IVS).

The calculation results using MP2/6-31G(d′)-determined geometries and HF/6-31G(d′)-determined frequencies are summarized in Table 5. TVR represents the sum of the contributions from translation, vibrations, and external rotations for S°_{298} and $C_p(T)$ values. Symmetry, number of optical isomers, and electronic spin are incorporated in estimation of S°_{298} as described in Table 5. Torsion frequency vibrations are omitted in these calculations; instead, contributions from internal rotation for S°_{298} and $C_p(T)$ values are calculated on the basis of rotational barrier heights and moments of inertia of the rotors using the method of Pitzer and Gwinn;[44] data on these parameters are listed in Table VS with internal rotor contributions noted in Table 5.

4.4. Energy Diagram for $C^{\bullet}H_2CHO + O_2$ Reaction System. The energy diagram for the $C^{\bullet}H_2CHO + O_2$ reaction system is illustrated in Figure 2, where enthalpies of formation are from CBSQ calculations in units of kilocalories per mole. The formyl methyl radical $C^{\bullet}H_2CHO$ ($\Delta H_f^{\circ}{}_{298}$ = 3.52 kcal/mol) adds to O_2 (E_a = 2.97) to form a $C(OO^{\bullet})H_2CHO$ peroxy radical with a 27.5 kcal/mol well depth. This peroxy radical can undergo dissociation back to reactants, decompose to products, $CH_2CO + HO_2$ via concerted HO_2 elimination with a barrier (E_a = 48.31), or isomerize via hydrogen shift (E_a = 20.25) to form a $C(OOH)H_2C^{\bullet}O$ isomer ($\Delta H_f^{\circ}{}_{298}$ = −19.64).

The $C(OOH)H_2C^{\bullet}O$ isomer can undergo β scission to products, $CH_2CO + HO_2$ (E_a = 23.53), decompose to $CO + C^{\bullet}H_2OOH$ ($C^{\bullet}H_2OOH$ rapidly dissociates to $CH_2O + OH$ with little or no barrier) (E_a = 10.32) via $T_2E(C^{\bullet}H_2OOH)$, decompose directly to $CO + CH_2O + OH$ (E_a = 16.80) via $T_2D(CO + CH_2O + OH)$, decompose to a diradical, $CH_2O^{\bullet}C^{\bullet}O + OH$ via simple RO−OH bond cleavage (E_a = 40.14), or isomerize via hydrogen shift (E_a = 18.88) to form a $C(OO^{\bullet})H_2CHO$ isomer.

TABLE 6: Comparison of $C^{\bullet}H_2CHO$, $CH_3C^{\bullet}(=O)$, and C_2H_5 (Kilocalories per Mole) with O_2

	$C.H_2CHO + O_2$	$CH_3C.(=O) + O_2$	$C_2H_5 + O_2$
well depth	27.5	35.5	35.3
H shift[a]	20.25	26.42	36.36
HO_2 elimination[a]	48.31	34.58	30.48

[a] H shift and HO_2 elimination for the $C(OO^{\bullet})H_2CHO$, $CH_3C(=O)OO^{\bullet}$, and C_2H_5OO.

TABLE 7: Input Parameters[a] and High-Pressure-Limit Rate Constants (k_∞)[b] for QRRK Calculations[c]

Input Parameters for QRRK Calculations with Master Equation Analysis for Falloff	high-pressure-limit rate constants		
		k_∞	
reaction	A	n	E_a (kcal/mol)
1 $C^{\bullet}H_2CHO + O_2 \rightarrow C(OO^{\bullet})H_2CHO$[d]	3.74E+07	1.55	3.12
−1 $C(OO^{\bullet})H_2CHO \rightarrow C^{\bullet}H_2CHO + O_2$[d]	2.54E+11	0.80	27.81
2 $C(OO^{\bullet})H_2CHO \rightarrow C(OOH)H_2C^{\bullet}O$[d]	1.04E+04	2.22	17.67
3 $C(OO^{\bullet})H_2CHO \rightarrow CH_2CO + HO_2$[d]	4.35E+08	1.76	48.24
4 $C(OOH)H_2C^{\bullet}O \rightarrow CO + CH_2O + OH$[d]	8.47E+10	2.04	10.10
5 $C(OOH)H_2C^{\bullet}O \rightarrow CH_2CO + HO_2$[d]	1.47E+10	0.65	23.82

[a] Geometric mean frequency [from CPFIT, ref 41: 740.8 cm^{-1} (7.239); 725.6 cm^{-1} (4.899); 2180.4 cm^{-1} (4.862). Lennard-Jones parameters: σ_{ij} = 5.19 Å, ϵ/k = 533.08 K, ref 62]. [b] Units of A factors and rate constants k are s^{-1} for unimolecular reactions and $cm^3/(mol\cdot s)$ for bimolecular reactions. [c] ΔE down of 1000 cal/mol is used, N_2 for bath gas. Units: k_1, $cm^3/(mol\cdot s)$; $k_{-1} \rightarrow k_5$: s^{-1}. [d] A is calculated using TST and entropy of transition state, $\Delta S^{\ddagger}_{298}$ from HF/6-31G(d′) (see Table VIS); E_a is from CBSQ calculation (see Table 5 and description for determination of E_a in Scheme 4). All parameters A, n, and E_a, are fit over the temperature range of 298−2000 K.

4.5. Comparison of $C^{\bullet}H_2CHO + O_2$, $CH_3C^{\bullet}O + O_2$, and $C_2H_5 + O_2$. The $C^{\bullet}H_2CHO + O_2$, $CH_3C^{\bullet}O + O_2$,[58] and $C_2H_5 + O_2$[30] reaction systems have significant differences. The $C^{\bullet}H_2CHO + O_2$ reaction system of this study has a lower well depth of 27.5 kcal/mol compared to $CH_3C^{\bullet}O + O_2$ and $C_2H_5 + O_2$, which have well depths of 35.5 and 35.3 kcal/mol, respectively.

The H-shift barriers in the $C(OO^{\bullet})H_2CHO$ and $CH_3C(=O)OO^{\bullet}$ peroxy radicals are both lower than those of concerted HO_2 elimination, whereas in $C_2H_5OO^{\bullet}$ direct HO_2 elimination has a lower barrier than the H shift.

The well depth and barriers of H shift and HO_2 elimination in the $C^{\bullet}H_2CHO$, $CH_3C^{\bullet}O$, and $C_2H_5^{\bullet}$ with O_2 reaction systems are compared in Table 6.

4.6. Analysis of the $C^{\bullet}H_2CHO + O_2$ Chemical Activation Reaction. QRRK calculations for $k(E)$ and master equation analysis for falloff are performed on this $C^{\bullet}H_2CHO + O_2$ reaction system to estimate rate constants and to determine important reaction paths as a function of temperature and

TABLE 8: Resulting Rate Constants in QRRK Calculations[a]

Calculated Reaction Parameters at $P = 0.01$ atm, $k = A(T/K)^n \exp(-E_a/RT)$ ($298 \le T/K \le 2000$)

reaction	A	n	E_a (kcal/mol)	k_{298}
1 $C^{\bullet}H_2CHO + O_2 \rightleftharpoons C(OO^{\bullet})H_2CHO$	1.58E+77	−21.90	19.35	6.68E+08
6 $C^{\bullet}H_2CHO + O_2 \rightleftharpoons CH_2CO + HO_2$	1.88E+05	2.37	23.73	5.43E−07
7 $C^{\bullet}H_2CHO + O_2 \rightleftharpoons CO + CH_2O + OH$	2.68E+17	−1.84	6.53	1.21E+08
8 $C^{\bullet}H_2CHO + O_2 \rightleftharpoons C(OOH)H_2C^{\bullet}O$	3.64E+65	−21.87	19.02	3.16E−03
2 $C(OO^{\bullet})H_2CHO \rightleftharpoons C(OOH)H_2C^{\bullet}O$	8.27E+30	−6.65	24.50	3.13E−04
3 $C(OO^{\bullet})H_2CHO \rightleftharpoons CH_2CO + HO_2$	2.05E+40	−13.31	52.15	1.35E−31
4 $C(OOH)H_2C^{\bullet}O \rightleftharpoons CO + CH_2O + OH$	2.36E+17	−2.95	8.10	1.37E+04
5 $C(OOH)H_2C^{\bullet}O \rightleftharpoons CH_2CO + HO_2$	1.12E+07	−3.76	21.68	6.99E−19

Calculated Reaction Parameters at $P = 0.1$ atm, $k = A(T/K)^n \exp(-E_a/RT)$ ($298 \le T/K \le 2000$)

reaction	A	n	E_a (kcal/mol)	k_{298}
1 $C^{\bullet}H_2CHO + O_2 \rightleftharpoons C(OO^{\bullet})H_2CHO$	3.88E+69	−18.84	19.24	7.33E+08
6 $C^{\bullet}H_2CHO + O_2 \rightleftharpoons CH_2CO + HO_2$	1.88E+05	2.37	23.73	5.43E−07
7 $C^{\bullet}H_2CHO + O_2 \rightleftharpoons CO + CH_2O + OH$	1.52E+20	−2.58	8.98	1.62E+07
8 $C^{\bullet}H_2CHO + O_2 \rightleftharpoons C(OOH)H_2C^{\bullet}O$	3.64E+58	−19.00	19.09	3.53E−03
2 $C(OO^{\bullet})H_2CHO \rightleftharpoons C(OOH)H_2C^{\bullet}O$	1.73E+26	−4.99	23.76	2.92E−04
3 $C(OO^{\bullet})H_2CHO \rightleftharpoons CH_2CO + HO_2$	5.72E+45	−14.00	52.20	6.80E−28
4 $C(OOH)H_2C^{\bullet}O \rightleftharpoons CO + CH_2O + OH$	2.38E+18	−2.95	8.10	1.37E+05
5 $C(OOH)H_2C^{\bullet}O \rightleftharpoons CH_2CO + HO_2$	1.10E+08	−3.76	21.68	6.92E−18

Calculated Reaction Parameters at $P = 1$ atm, $k = A(T/K)^n \exp(-E_a/RT)$ ($298 \le T/K \le 2000$)

reaction	A	n	E_a (kcal/mol)	k_{298}
1 $C^{\bullet}H_2CHO + O_2 \rightleftharpoons C(OO^{\bullet})H_2CHO$	7.80E+59	−15.40	17.65	7.04E+08
6 $C^{\bullet}H_2CHO + O_2 \rightleftharpoons CH_2CO + HO_2$	2.51E+05	2.33	23.80	5.15E−07
7 $C^{\bullet}H_2CHO + O_2 \rightleftharpoons CO + CH_2O + OH$	1.65E+19	−2.22	10.34	1.37E+06
8 $C^{\bullet}H_2CHO + O_2 \rightleftharpoons C(OOH)H_2C^{\bullet}O$	6.65E+48	−15.55	17.46	3.51E−03
2 $C(OO^{\bullet})H_2CHO \rightleftharpoons C(OOH)H_2C^{\bullet}O$	9.03E+19	−2.92	22.17	2.97E−04
3 $C(OO^{\bullet})H_2CHO \rightleftharpoons CH_2CO + HO_2$	4.16E+55	−15.76	55.08	1.68E−24
4 $C(OOH)H_2C^{\bullet}O \rightleftharpoons CO + CH_2O + OH$	2.51E+19	−2.95	8.11	1.42E+06
5 $C(OOH)H_2C^{\bullet}O \rightleftharpoons CH_2CO + HO_2$	9.20E+08	−3.73	21.63	7.43E−17

Calculated Reaction Parameters at $P = 10$ atm, $k = A(T/K)^n \exp(-E_a/RT)$ ($298 \le T/K \le 2000$)

reaction	A	n	E_a (kcal/mol)	k_{298}
1 $C^{\bullet}H_2CHO + O_2 \rightleftharpoons C(OO^{\bullet})H_2CHO$	3.05E+50	−12.20	15.63	6.86E+08
6 $C^{\bullet}H_2CHO + O_2 \rightleftharpoons CH_2CO + HO_2$	7.05E+07	1.63	25.29	2.16E−07
7 $C^{\bullet}H_2CHO + O_2 \rightleftharpoons CO + CH_2O + OH$	8.95E+13	−0.60	10.12	1.11E+05
8 $C^{\bullet}H_2CHO + O_2 \rightleftharpoons C(OOH)H_2C^{\bullet}O$	4.80E+38	−12.14	14.96	4.72E−03
2 $C(OO^{\bullet})H_2CHO \rightleftharpoons C(OOH)H_2C^{\bullet}O$	1.43E+16	−1.67	21.21	2.94E−04
3 $C(OO^{\bullet})H_2CHO \rightleftharpoons CH_2CO + HO_2$	1.12E+61	−16.04	60.01	2.23E−23
4 $C(OOH)H_2C^{\bullet}O \rightleftharpoons CO + CH_2O + OH$	4.16E+20	−3.02	8.24	1.27E+07
5 $C(OOH)H_2C^{\bullet}O \rightleftharpoons CH_2CO + HO_2$	2.09E+09	−3.55	21.22	9.46E−16

[a] Units of A factors and rate constants k are s^{-1} for unimolecular reactions and $cm^3/(mol \cdot s)$ for bimolecular reactions.

pressure. Table 7 presents high-pressure-limit kinetic parameters used as input data, and Table 8 presents results versus temperature and pressure.

Rate constants at 1 atm pressure versus $1000/T$ are illustrated in Figure 3. Stabilization [$C(OO^{\bullet})H_2CHO$] is important below 500 K, with reverse dissociation and $CO + CH_2O + OH$ products important above 1000 K. The ketene + HO_2 product set via direct HO_2 elimination is also important above 1500 K.

Plots of calculated rate constants for $C^{\bullet}H_2CHO + O_2$ at 298 K versus pressure are illustrated in Figure 4. Stabilization is the dominant path above 0.1 atm, whereas stabilization, reverse dissociation, and $CO + CH_2O + OH$ products are important below 0.01 atm.

Rate constants at 1000 K versus pressure are illustrated in Figure 5. Reverse dissociation and $CO + CH_2O + OH$ products are most important at both high and low pressures. Stabilization decreases as pressure is decreased.

4.7. Abstraction of a Hydrogen from the −CHO Group of $C^{\bullet}H_2CHO$ by O_2.

$$C^{\bullet}H_2CHO + {}^3O_2 \rightarrow CH_2CO + HO_2 \ (\Delta H_f^{\circ}{}_{rxn,298} = -12.79 \text{ kcal/mol in CBSQ}) \quad (2)$$

A transition state for direct abstraction of a hydrogen from the −CHO group of $C^{\bullet}H_2CHO$ by O_2 to form ketene + HO_2 is identified with a barrier of ~29 kcal/mol at the CBSQ level. (This TS is calculated as a doublet.) This barrier seems to be high for a reaction that is this exothermic, so further calculations were performed. The species structures and the barrier are further calculated using the recently published KMLYP density functional method[63] with the /6-311G(d,p) basis set. The barrier is calculated relative to the reactants and relative to the HO_2 elimination transition state [$T_2E(HO_2)$]. Comparison of the two calculation results for the three methods (B3LYP, KMLYP, and CBSQ) is given in Scheme 5. The barrier of 28.8 kcal/mol at CBSQ is similar in both comparisons. This value is 4.3 kcal/mol lower than the value from KMLYP and 4.1 kcal/mol higher that from B3LYP. Kang et al.[63] reported comparisons between the B3LYP barriers and experiment showing that B3LYP is less accurate than KMLYP in estimating barriers and that it has a tendency to underestimate barriers as reported in several studies.[64−66] The value at CBSQ level is chosen.[23,24,38]

The barrier is determined to be high in all of the calculation methods. The high barrier is interpreted as being due to the noninitiation of the new C═C Π bond in the TS structure, where

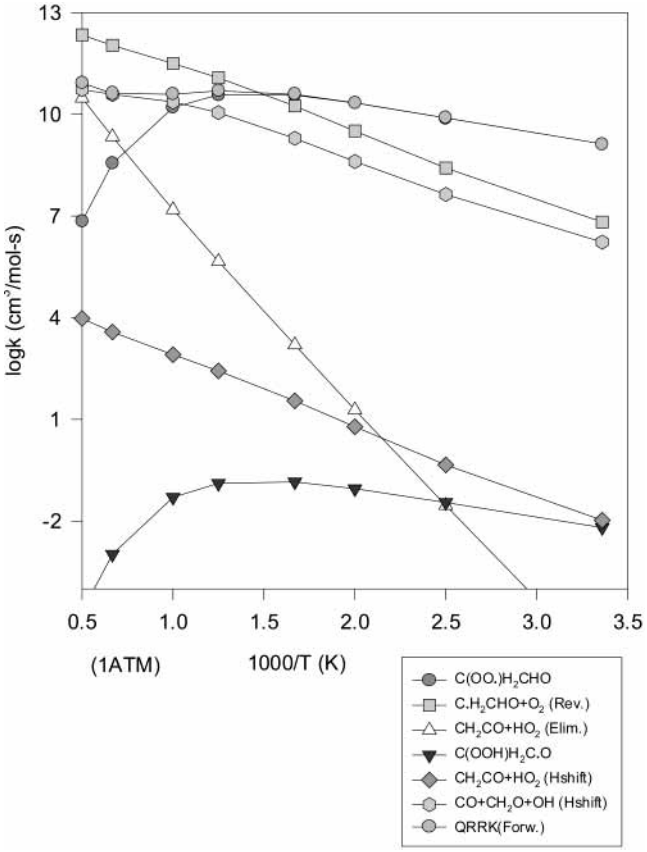

Figure 3. C•H$_2$CHO + O$_2$ → products *k* versus 1000/*T* at 1 atm.

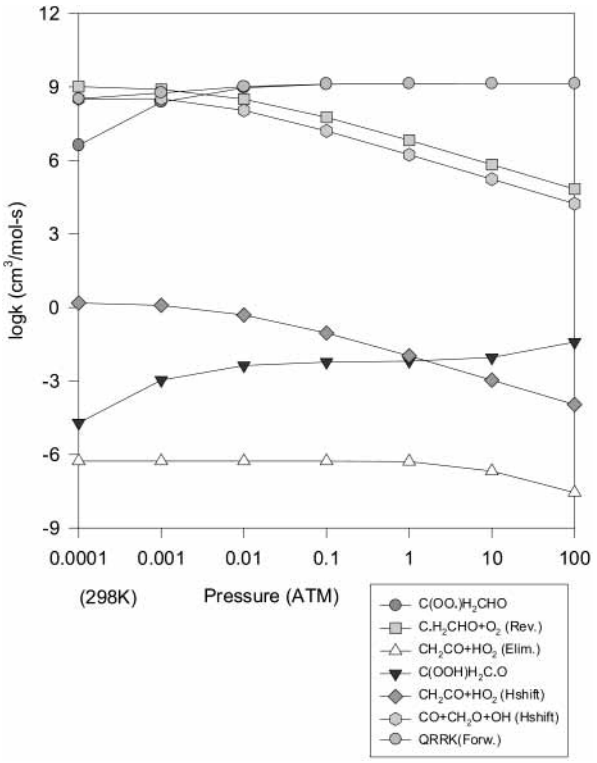

Figure 4. C•H$_2$CHO + O$_2$ → products *k* versus pressure at 298 K.

some rearrangement is required to form the ketene structure, for this direct hydrogen abstraction by O$_2$ from the −CH(═O). The forming C═C bond is 1.42 Å in the transition state structure and is 1.47 Å in the stable C•H$_2$CHO radical.

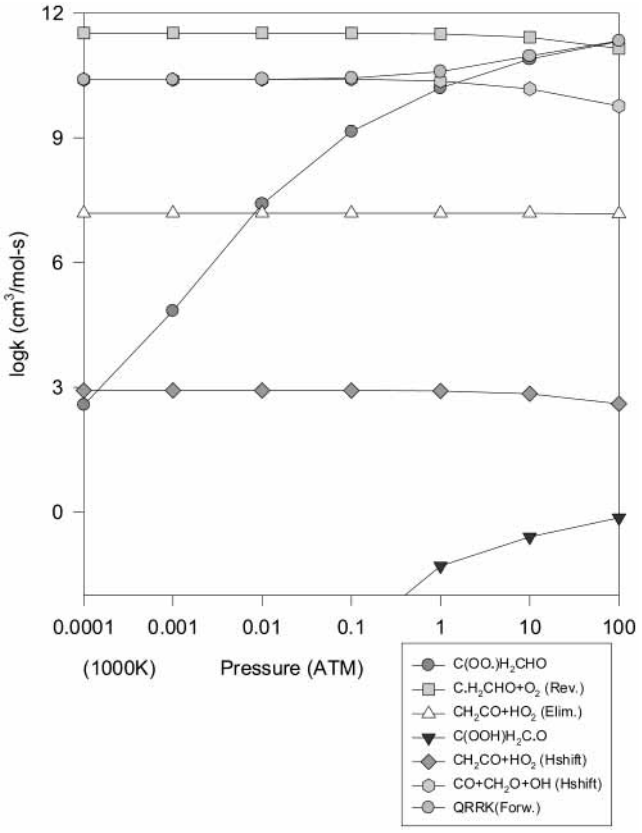

Figure 5. C•H$_2$CHO + O$_2$ → products *k* versus pressure at 1000 K.

SCHEME 5: Comparison of Activation Energies[a]

Units (kcal/mol)	(a) Ea	(b) Ea
CBSQ	28.84	28.61
KMLYP/6-311G(d,p)	33.10	25.55
B3LYP/6-31G(d)	24.67	15.76

[a] E_a values are calculated from (a) C•H$_2$CHO + ^{3}O$_2$ → TS (bimolecular reaction) and (b) relative to T$_2$E(HO$_2$) (unimolecular reaction).

This direct abstraction channel to form ketene + HO$_2$ is not competitive with the chemical activation C•H$_2$CHO by O$_2$ (association) rate constant to the same product set below 1500 K at 1 atm.

4.8. Unimolecular Dissociation of Formyl Methyl Peroxy and Acetyl Hydroperoxide Radicals. Stabilization of the adducts is observed to be important at lower temperature and moderate pressure conditions. Important dissociation products of the adducts and the rate constants are, therefore, of value.

(1) C(OO•)H$_2$CHO Dissociation Reaction. Plots of rate constants for C(OO•)H$_2$CHO dissociation at 1 atm pressure versus 1000/*T* and of rate constants at 298 and 1000 K versus pressure are illustrated in the Supporting Information (Figures 1S, 2S, and 3S, respectively). C•H$_2$CHO + O$_2$ and CO + CH$_2$O + OH products via H shift are important above 500 K at both high and low pressures. CO + CH$_2$O + OH products via H shift is the dominant path below 500 K, at which the ketene + HO$_2$ products increase as temperature is increased at 1 atm pressure.

(2) C(OOH)H$_2$C•O Dissociation Reaction. Rate constants for C(OOH)H$_2$C•O dissociation at 1 atm pressure versus 1000/*T* and rate constants at 298 and 1000 K versus pressure are illustrated in the Supporting Information (Figures 4S, 5S, and 6S, respectively). The CO + CH$_2$O + OH product set is most

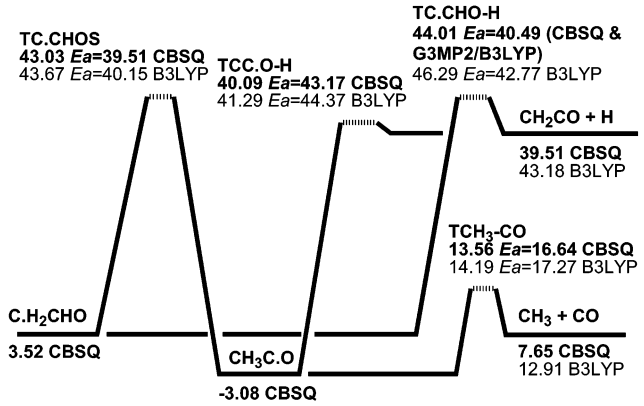

Figure 6. Potential energy (kcal/mol) diagram of acetyl and formyl methyl radical unimolecular isomerization/dissociations.

important at both high and low temperatures and decrease as temperature is decreased. Isomerization to $C(OO^{\bullet})H_2CHO$ shows falloff above 600 K. At 298 and 1000 K, the CO + CH_2O + OH product set is the dominant path at both high and low pressures.

4.9. Formyl Methyl Radical Unimolecular Dissociation. The energy diagram for formyl methyl radical unimolecular dissociation is illustrated in Figure 6. The formyl methyl radical, $C^{\bullet}H_2CHO$, can undergo β scission to products, CH_2CO + H (E_a = 40.49), or isomerize via H shift (E_a = 39.51) to form the slightly lower energy $CH_3C^{\bullet}O$ isomer. The barriers of these two channels are similar.

This $CH_3C^{\bullet}O$ isomer can decompose to CH_3 + CO (E_a = 16.64), undergo β scission to products, CH_2CO + H (E_a = 43.17), or isomerize via H shift (E_a = 46.11) to form the $C^{\bullet}H_2CHO$ isomer. The barrier of $CH_3C^{\bullet}O$ decomposition to CH_3 + CO is 26.5 kcal/mol lower than the barrier for β scission to products, CH_2CO + H; thus, the CH_3 + CO product set is the dominant path for $CH_3C^{\bullet}O$ dissociation.

4.10. Detailed Mechanism of Formyl Methyl Radical Oxidation Reactions. A small detailed mechanism including the reactions evaluated in this study is assembled and given in Table 9. The mechanism consists of 72 reactions and 31 species with each elementary reaction evaluated and referenced. The Chemkin II integrator code[67] is used to model typical low-pressure flow reactor conditions[14] in this study on the formyl methyl radical + O_2 reaction system. The acetyl radical + O_2 reaction system was previously modeled under similar conditions.[58] Abstraction reactions by O, H, OH, HO_2, O_2, and CH_3 radicals are taken from evaluated literature whenever possible. A procedure from Dean and Bozzelli[51] is used to estimate abstraction rate constants by H, HO_2, CH_3, and $CH_3C(=O)$-$OO^{\bullet}$ radicals when no literature data are available.

The reactions of CH_3CHO + OH → $CH_3C^{\bullet}O$ and → $C^{\bullet}H_2CHO$ + H_2O are analyzed to model these typical low-pressure flow reactor conditions: 0−0.01 s, 300 K, and 3 Torr. The reaction with no O_2 added (mole fraction: CH_3CHO = 1.2×10^{-4}, OH = 3.6×10^{-6}) shows 99% $CH_3C^{\bullet}O$, acetyl radical, and 1% $C^{\bullet}H_2CHO$, formyl methyl radical, at 0.01 s via OH abstraction paths. This is in agreement with the data of Michael et al.[15] and Slagle et al.[16]

Data on concentration versus time for reaction conditions similar to those above [reaction time (0−1.0 s), plus 3 Torr of O_2 (mole fraction = 9.1×10^{-4})] are illustrated in Figure 7.

TABLE 9: Detailed Mechanism

reaction		*A*	*n*	E_a	ref	reaction		*A*	*n*	E_a	ref
CH_3CHO	$= CH_3 + HCO$	6.99E+44	−9.82	88320	a	$CH_3 + O_2$	$= CH_3OO$	1.99E+31	−6.72	4212	f
CH_3CHO	$= CH_3C^{\bullet}O + H$	7.50E+44	−11.49	92652	a	CH_3OO	$= CH_2O + OH$	1.99E+20	−7.76	47315	a
$CH_3CHO + O_2$	$= CH_3C^{\bullet}O + HO_2$	3.01E+13	0.0	39143	b	$CH_3 + CH_2O$	$= HCO + CH_4$	5.54E+03	2.81	5862	g
HCO	$= H + CO$	7.94E+17	−3.51	16326	a	$CH_3 + HO_2$	$= CH_3O + OH$	1.81E+13	0.0	0	b
$CH_3CHO + OH$	$= C^{\bullet}H_2CHO + H_2O$	4.31E+11	0.0	1000	c	CH_3O	$= CH_2O + H$	6.13E+28	−5.65	31351	f
$CH_3CHO + H$	$= C^{\bullet}H_2CHO + H_2$	2.4E+8	1.5	2103	d	$CH_3O + HO_2$	$= CH_2O + H_2O_2$	3.01E+11	0.0	0	g
$CH_3CHO + O$	$= C^{\bullet}H_2CHO + OH$	5.85E+12	0.0	1808	b	$CH_2O + O$	$= OH + HCO$	1.81E+13	0.0	3080	g
$CH_3CHO + HO_2$	$= C^{\bullet}H_2CHO + H_2O_2$	1.4E+4	2.69	14068	d	$CH_2O + H$	$= H_2 + HCO$	2.29E+10	1.05	3279	b
$CH_3CHO + CH_3$	$= C^{\bullet}H_2CHO + CH_4$	8.1E+5	1.87	5251	d	$CH_2O + OH$	$= H_2O + HCO$	3.44E+09	1.18	−447	b
$C^{\bullet}H_2CHO + O_2$	$= C(OO^{\bullet})H_2CHO$	8.22E+90	−27.02	21062	a	$HCO + O_2$	$= CO + HO_2$	6.25E+15	−1.15	2018	f
$C^{\bullet}H_2CHO + O_2$	$= CH_2CO + HO_2$	1.88E+05	2.37	23728	a	$HCO + O_2$	$= CO_2 + OH$	5.45E+14	−1.15	2018	f
$C^{\bullet}H_2CHO + O_2$	$= C(OOH)H_2C^{\bullet}(=O)$	6.62E+73	−26.06	20125	a	$CO + O$	$= CO_2$	6.17E+14	0.0	3001	g
$C^{\bullet}H_2CHO + O_2$	$= CH_2CO + HO_2$	1.15E−03	2.21	3493	a	$CO + OH$	$= CO_2 + H$	6.32E+06	1.5	−497	g
$C^{\bullet}H_2CHO + O_2$	$= CO + CH_2O + OH$	1.18E+15	−1.16	5109	a	$CO + HO_2$	$= CO_2 + OH$	1.51E+14	0.0	23650	g
$C^{\bullet}H_2CHO + O_2$	$= CH_2O^{\bullet}C^{\bullet}O + OH$	3.24E−01	2.43	14700	a	$CO + O_2$	$= CO_2 + O$	2.53E+12	0.0	47693	g
$C(OO^{\bullet})H_2CHO$	$= C^{\bullet}H_2CHO + O_2$	4.45E+74	−21.35	39750	a	$H + O_2 + M$	$= HO_2 + M$	1.41E+18	−0.8	0	b
$C(OO^{\bullet})H_2CHO$	$= CH_2CO + HO_2$	3.26E+49	−19.88	53147	a	$H + O_2$	$= OH + O$	1.99E+14	0.0	16802	b
$C(OO^{\bullet})H_2CHO$	$= CH_2(OOH)C^{\bullet}(=O)$	8.57E+32	−7.48	24373	a	$OH + OH$	$= O + H_2O$	1.51E+09	1.14	99	b
$C(OOH)H_2C^{\bullet}(=O)$	$= CH_2CO + HO_2$	9.55E+02	−4.58	22116	a	$H_2 + OH$	$= H_2O + H$	1.02E+08	1.6	3300	b
$C(OOH)H_2C^{\bullet}(=O)$	$= CO + CH_2O + OH$	1.39E+18	−3.32	8482	a	$H + OH + M$	$= H_2O + M$	2.21E+22	−2.0	0	b
$C(OOH)H_2C^{\bullet}(=O)$	$= CH_2O^{\bullet}C^{\bullet}O + OH$	8.21E−05	−5.22	36056	a	$O + HO_2$	$= OH + O_2$	1.75E+13	0.0	−397	h
$C(OOH)H_2C^{\bullet}(=O)$	$= C(OO^{\bullet})H_2CHO$	9.60E+04	−3.41	14091	a	$OH + HO_2$	$= H_2O + O_2$	1.45E+16	−1.0	0	g
$CH_2O^{\bullet}C^{\bullet}O$	$= CH_2O + CO$	2.02E+10	−1.08	2552	a	$H + HO_2$	$= OH + OH$	1.69E+14	0.0	874	g
$C(OOH)H_2C^{\bullet}(=O)+O_2$	$= C(OOH)H_2C(=O)OO^{\bullet}$	3.38E+68	−21.47	7828	a	$H + HO_2$	$= H_2 + O_2$	6.62E+13	0.0	2126	g
$C(OOH)H_2C^{\bullet}(=O) + O_2$	$= CHOC(=O)OOH + OH$	2.06E+16	−1.43	1083	a	$H + HO_2$	$= H_2O + O$	3.01E+13	0.0	1721	b
$C(OOH)H_2C(=O)OO^{\bullet}$	$= C(OOH)H_2C^{\bullet}(=O) + O_2$	4.99E+50	−14.75	37753	a	$H + O + M$	$= OH + M$	4.71E+18	−1.0	0	g
$C(OOH)H_2C(=O)OO^{\bullet}$	$= CHOC(=O)OOH + OH$	1.61E+41	−9.97	26200	a	$H_2O_2 + M$	$= OH + OH + M$	1.21E+17	0.0	45507	b
$CH_3C^{\bullet}O$	$= CH_2CO + H$	2.33E−23	1.64	38980	a	$H_2O_2 + OH$	$= H_2O + HO_2$	1.75E+12	0.0	318	h
$CH_3C^{\bullet}O$	$= CH_3 + CO$	4.87E+06	0.33	12525	a	$H_2O_2 + O$	$= OH + HO_2$	9.63E+06	2.0	3974	g
$CH_3C^{\bullet}O$	$= C^{\bullet}H_2CHO$	7.10E−25	1.48	39974	a	$H_2O_2 + H$	$= OH + H_2O$	2.41E+13	0.0	3974	g
$C^{\bullet}H_2CHO$	$= CH_2CO + H$	1.43E+38	−8.75	46719	a	$H_2O_2 + H$	$= HO_2 + H_2$	4.82E+13	0.0	7949	g
$C^{\bullet}H_2CHO$	$= CH_3C^{\bullet}O$	5.84E+38	−9.08	46719	a	$CH_4 + HO_2$	$= H_2O_2 + CH_3$	9.04E+12	0.0	24641	b
$C(OO^{\bullet})H_2CHO + NO$	$= C(O^{\bullet})H_2CHO + NO_2$	1.26E+12	0.0	1133	e	$2HO_2$	$= 2OH + O_2$	1.00E+12	0.0	11500	f
$C(O^{\bullet})H_2CHO$	$= CH_2O + HCO$	8.72E+22	−4.9	12378	a	$HO_2 + HO_2$	$= H_2O_2 + O_2$	1.87E+12	0.0	1540	b
$C(O^{\bullet})H_2CHO$	$= CHOCHO + H$	2.94E+13	−2.2	28503	a	$H + H + M$	$= H_2 + M$	5.44E+18	−1.3	0	g
$CH_3 + O_2$	$= CH_2O + OH$	2.61E+08	1.01	12487	f	$O + H_2$	$= OH + H$	5.12E+04	2.67	6285	b

[a] From QRRK calculations (3 Torr, 298−2000 K). [b] Reference 68. [c] Reference 69. [d] Estimated in this study. [e] Reference 70. [f] Reference 71. [g] Reference 72. [h] Reference 73.

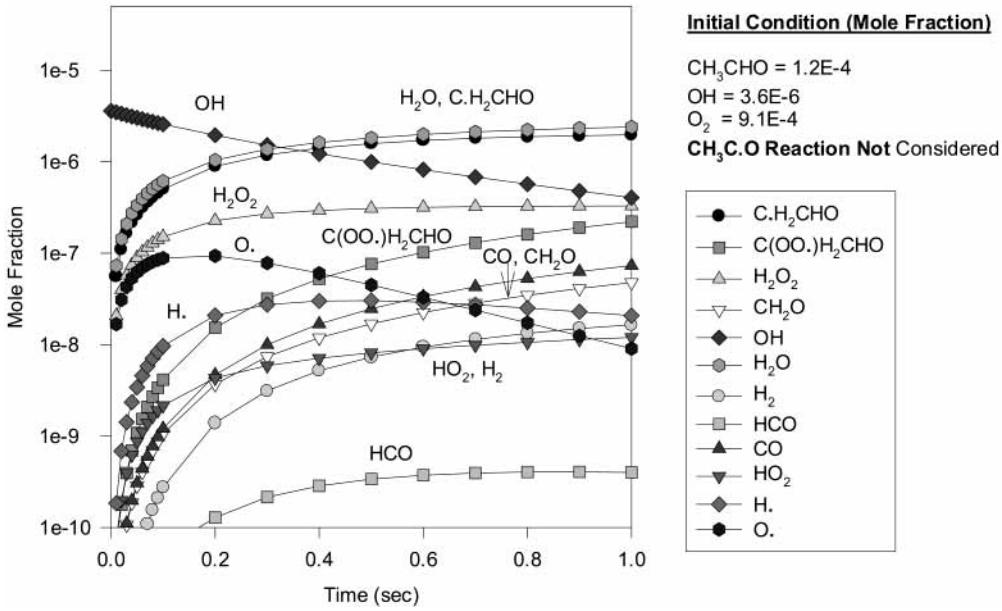

Figure 7. Chemkin kinetic calculation: concentration versus time (OH abstraction of the carbonyl H atom is turned off in these model runs in order to observe the formyl methyl radical formation and its reactions).

Formation of $CH_3C^{\bullet}O$ is not included here as we focus on $C^{\bullet}H_2CHO$ ($CH_3C^{\bullet}O$ is discussed in ref 58). $C(OO^{\bullet})H_2CHO$, CO, and CH_2O are the major products; these result from formyl methyl radical reaction with O_2. In the mechanism the diradical $CH_2O^{\bullet}C^{\bullet}O$ dissociates to $CH_2O + CO$. Under these conditions (3 Torr of O_2), we observe that 11% of the OH radical is regenerated through the formyl methyl radical with O_2 reaction.

Reaction analysis at atmospheric pressure is also modeled with reaction time (0 − 1.0 s) at 300 K (mole fractions: $N_2 = 0.8$, $O_2 = 0.2$, $CH_3CHO = 1.0 \times 10^{-4}$, and $OH = 1.0 \times 10^{-7}$). The product ratio is determined as 34.12% [$C(OO^{\bullet})H_2CHO$/OH]. The concentration of $CO + CH_2O + OH$ product set is $\sim 10^3$ times lower to $C(OO^{\bullet})H_2CHO$.

4.11. Comparison of $C^{\bullet}H_2CHO + O_2$ with Unimolecular Dissociation of $C^{\bullet}H_2CHO$. The competition between unimolecular dissociation of $C^{\bullet}H_2CHO \rightarrow CH_2CO + H$ versus association of $C^{\bullet}H_2CHO$ with O_2 as a function of reactor temperature is considered. We utilize the above mechanism for this evaluation because the reaction system is complex, and it involves reactions of chemical activated and stabilized $C(OO^{\bullet})H_2CHO$.

Several reaction condition sets are evaluated, one is the low-pressure flow reactor above[14] (1.0 s reaction time with CH_3CHO at 1.2×10^{-4}, $OH = 3.6 \times 10^{-6}$, and $O_2 = 9.1 \times 10^{-4}$ mole fractions). The second condition set is 1 atm pressure; both condition sets are over varied temperature. The fraction of formyl methyl that reacts with O_2 versus unimolecular dissociation is summarized in Scheme 6, which shows that the two reaction processes, oxidation and unimolecular dissociation, are competitive around 800 K at 3 Torr. The unimolecular dissociation channel accounts for >80% of the reaction at 900 K at 3 Torr.

The third condition set considers the competition between oxidation and dissociation at concentrations more relative to combustion [mole fractions: $C^{\bullet}H_2CHO = 1.0 \times 10^{-5}$, $O_2 = 0.15$, $N_2 = 0.80$, and CH_4 (fuel) = 0.05]. Plots of concentration versus time for 10 ns, at 900 K and 1 atm, are illustrated in Figure 8. The $C^{\bullet}H_2CHO$ radicals decrease slowly with time, from the oxidation with effectively no unimolecular dissociation. At 0.1 s time, the ratio of oxidation to unimolecular dissociation

SCHEME 6: Fraction of Oxidation and Dissociation of Formyl Methyl Radical[a]

T / %	Oxidation		Dissociation	
	3 Torr	1 atm	3 Torr	1 atm
600K	99.9	99.0	0.1	1.0
650K	99.2	86.7	0.8	13.3
700K	95.3	39.8	4.7	60.2
750K	81.3	8.7	18.7	91.3
800K	53.6	1.8	46.4	98.2
850K	27.0	0.5	73.0	99.5
900K	12.1	0.1	87.9	99.9
950K	5.4	0.1	94.6	99.9
1000K	2.6	0.0	97.4	100.0

[a] $t = 1.0$ s; mole fraction: $CH_3CHO = 1.2 \times 10^{-4}$, $OH = 3.6 \times 10^{-6}$, and $O_2 = 9.1 \times 10^{-4}$.

products, $CO + CH_2O + OH/CH_2CO + H$ is 42:1. The major products are stabilized $C(OO^{\bullet})H_2CHO$, CO, CH_2O, and OH, which result from formyl methyl radical reaction with O_2. The $C(OO^{\bullet})H_2CHO$ has a barrier to $C^{\bullet}H_2CHO + O_2$ of only 27.5 kcal/mol, and it dissociates rapidly at this temperature. It is not a highly stable product.

Products are illustrated in Figure 9 for reaction at 1100 K, 1 atm, and short times to evaluate initial reactor paths. The major species are CO, CH_2O, OH, CH_2CO, H, and $C(OO^{\bullet})H_2CHO$; these result from both formyl methyl radical reaction with O_2 and $C^{\bullet}H_2CHO$ unimolecular dissociation to $CH_2CO + H$. Above 1200 K, the major products are ketene and H from the unimolecular dissociation. The oxidation and dissociation channels are competitive at ~1100 K under these conditions. Ratios of the product sets are summarized in Scheme 7 at varied temperature. These data are in reasonable agreement with the relative unimolecular rate constants, where $[O_2]$ was included in the bimolecular rate constant for $C^{\bullet}H_2CHO + O_2$ association at these conditions (Tables VIIS and VIIIS). Similar trends are observed for longer times.

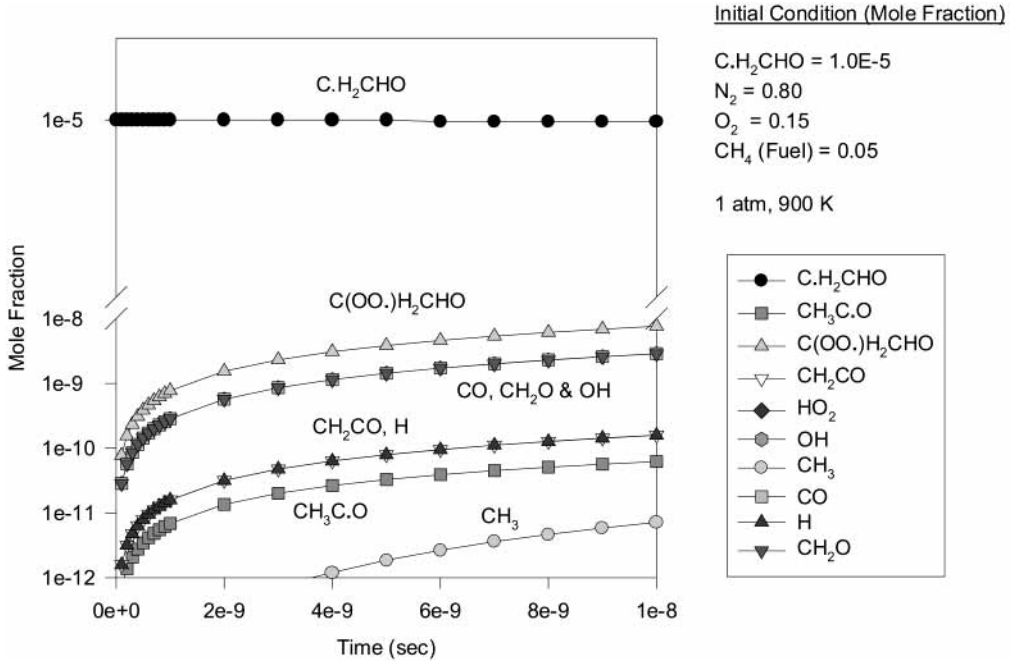

Figure 8. Chemkin kinetic calculation: concentration versus time.

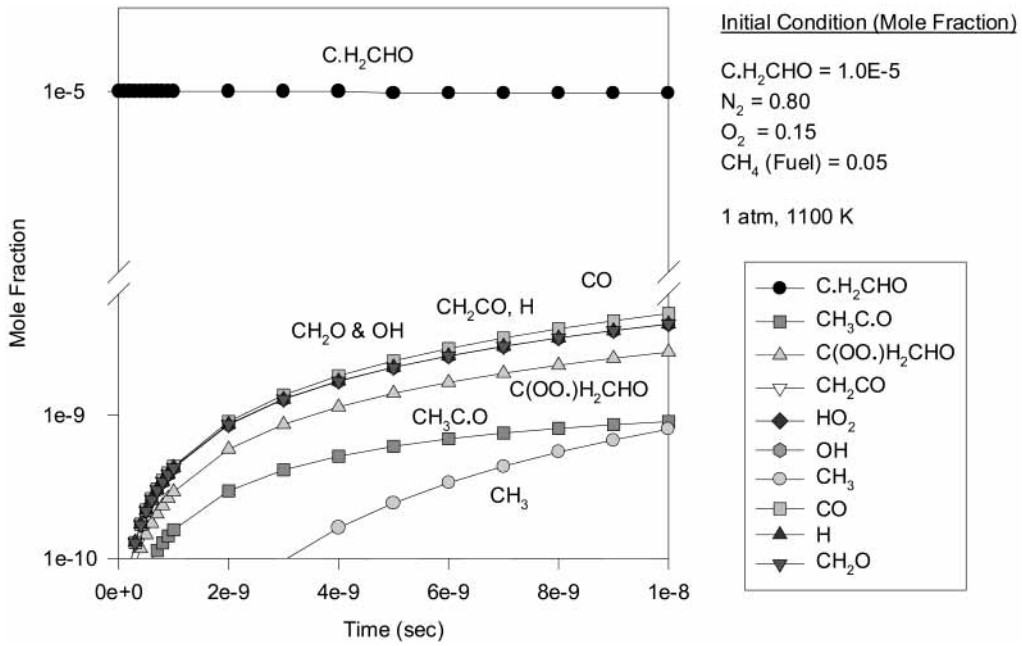

Figure 9. Chemkin kinetic calculation: concentration versus time.

5. Summary

Thermochemical properties of stable radicals and transition states on the $C^{\bullet}H_2CHO + O_2$ reaction system are calculated using density functional and ab initio methods. Enthalpies of formation ($\Delta H_f^\circ{}_{298}$) are determined using isodesmic reactions at the CBSQ level. Entropies ($S^\circ{}_{298}$) and heat capacities [$C_p(T)$] include internal rotor contributions. The $C^{\bullet}H_2CHO + O_2$ system is found to have a lower well depth of 27.5 kcal/mol compared to $CH_3C^{\bullet}O + O_2$ and $C_2H_5^{\bullet} + O_2$, which have well depths of 35.5 and 35.3 kcal/mol, respectively. The H shift and the HO_2 elimination barriers are also significantly different from those of ethyl and acetyl radical with O_2 reactions. Reaction paths and kinetics are analyzed on the $C^{\bullet}H_2CHO + O_2$ reaction system using QRRK for $k(E)$ and master equation for falloff. Reaction to products is evaluated versus both pressure and temperature.

Major reaction paths at 1 atm pressure are stabilization of the peroxy adduct [$C(OO^{\bullet})H_2CHO$] below 500 K, with reverse dissociation and $CO + CH_2O + OH$ products via H shift important at >1000 K.

A detailed reaction mechanism is constructed that includes pressure dependence for the formyl methyl radical reaction with O_2. The mechanism is also used to compare the competition between formyl methyl radical decomposition and reaction with O_2 versus temperature.

Acknowledgment. We acknowledge the U.S. EPA Northeast Regional Research Center and the U.S. EPA Airborne Organics Research Center for funding. We thank to C. Sheng for the SMCPS program.

SCHEME 7: Fraction of Oxidation and Dissociation of Formyl Methyl Radical[a]

T / %	Oxidation	Dissociation	Ratio
900K	94.8	5.2	0.1
1000K	78.3	21.7	0.3
1100K	50.0	50.0	1.0
1200K	26.2	73.8	2.8
1250K	18.6	81.4	4.4
1300K	13.2	86.8	6.6
1400K	7.0	93.0	13.2
1500K	4.0	96.0	23.8
1600K	2.5	97.5	39.1

(Ratio: Dissociation/Oxidation)

[a] t = 10 ns, pressure = 1 atm, mole fraction: $C^{\bullet}H_2CHO = 1.0 \times 10^{-5}$, $O_2 = 0.15$, $N_2 = 0.80$, and CH_4(fuel) = 0.05.

Nomenclature for Molecules

C carbon with hydrocarbons assumed to satisfy respective valance
T transition state
• radical site
= double bond
— bond (leaving/formed)

Supporting Information Available: Plots of rate constants at 1 atm pressure versus 1000/T and at 298 and 1000 K versus pressure for formyl methyl peroxy and acetyl hydroperoxide radical dissociation (Figures 1S−6S); table of geometries for intermediate radicals and transition states (Table 1S); tables of total energies, zero-point vibrational energies, and thermal corrections for CBSQ calculation and vibrational frequencies and moments of inertia at the HF/6-31G(d′) level of calculation (Tables IIS, IIIS, and IVS); table of rotational barriers for internal rotors (Table VS); tables of thermochemical analysis for reactions and ratio of rate constants and ratio of high-pressure-limit rate constants between unimolecular dissociation of $C^{\bullet}H_2CHO$ versus association of $C^{\bullet}H_2CHO$ with O_2 (Tables VIS, VIIS, and VIIIS). This material is available free of charge via the Internet at http://pubs.acs.org.

References and Notes

(1) Benson, S. W. *Thermochemical Kinetics*; Wiley: New York, 1976.
(2) Slagle, I. R.; Ratajaczak, E.; Gutman, D. J. *J. Phys. Chem.* **1986**, *90*, 402.
(3) Bozzelli, J. W.; Dean, A. M. *J. Phys. Chem.* **1993**, *97*, 4427.
(4) Chang, A. Y.; Bozzelli, J. W.; Dean, A. M. *Int. J. Res. Phys. Chem. Chem. Phys. (Z. Phys. Chem.)* **2000**, *214*, 1533.
(5) Mebel, A. M.; Diau, E. W. G.; Lin, M. C.; Morokuma, K. *J. Am. Chem. Soc.* **1996**, *118*, 9759.
(6) Bozzelli, J. W.; Sheng, C. *J. Phys. Chem. A* **2002**, *106*, 1113.
(7) Sebbar, N.; Bockhorn, H.; Bozzelli, J. W. *Phys. Chem. Chem. Phys.* **2002**, *4*, 3691.
(8) Olzmann, M.; Kraka, E.; Cremer, R.; Gutbrod, R.; Andersson, S. *J. Phys. Chem. A* **1997**, *101*, 9421.
(9) Tuazon, E. C.; Aschmann, S. M.; Arey, J.; Atkinson, R. *Environ. Sci. Technol.* **1997**, *31*, 3004.
(10) Atkinson, R.; Aschmann, S. M. *Environ. Sci. Technol.* **1993**, *27*, 1357.
(11) Sehested, I.; Christensen, L. K.; Nielsen, O. J.; Wallington, T. J. *Int. J. Chem. Kinet.* **1998**, *30*, 913.
(12) Atkinson, R.; Baulch, D. L.; Cox, R. A.; Hampson, R. F., Jr.; Kerr, J. A.; Troe, J. *J. Phys. Chem. Ref. Data* **1989**, *18*, 881.
(13) Bartels, M.; Hoyermann, K. *An. Asoc. Quim. Argent.* **1985**, *73*, 253.
(14) Tyndall, G. S.; Staffelbach, T. A.; Orlando, J. J.; Calvert, J. G. *Int. J. Chem. Kinet.* **1995**, *27*, 1009.
(15) Michael, J. V.; Keil, D. G.; Klemm, R. B. *J. Chem. Phys.* **1985**, *83*, 1630.
(16) Slagle, I. R.; Gutman, D. *J. Am. Chem. Soc.* **1982**, *104*, 4741.
(17) Alvarez-Idaboy, J. R.; Mora-Diez, N.; Boyd, R. J.; Vivier-Bunge, A. *J. Am. Chem. Soc.* **2001**, *123*, 2018.
(18) Aloisio, S.; Francisco, J. S. *J. Phys. Chem. A* **2000**, *104*, 3211.
(19) Zhu, L.; Johnston, G. *J. Phys. Chem.* **1995**, *99*, 15114.
(20) Stewart, J. J. P. *MOPAC 6.0*; Frank J. Seiler Research Laboratory, U.S. Air Force Academy: Colorado Spring, CO, 1990.
(21) Frisch, M. J.; Truck, G. W.; Head-Gordon, M.; Gill, P. M. W.; Wong, M. W.; Foresman, J. B.; Johnson, B. G.; Schelgel, H. B.; Robb, M. A.; Peplogle, E. S.; Gromperts, R.; Andres, J. L.; Raghavachari, K.; Binkley, J, S.; Gonzalez, C.; Martin, R. L.; Fox, D. J.; Defrees, D. J.; Baker, J.; Stewart, J. J. P.; Pople, J. A. *Gaussian 94*, revision C.2; Gaussian Inc.: Pittsburgh, PA, 1995.
(22) Petersson, G. A.; Bennett, A.; Tensfeldt, T. G.; Al-Laham, M. A.; Shirley, W. A.; Mantzaris, J. *J. Chem. Phys.* **1988**, *89*, 2193.
(23) Petersson, G. A.; Tensfeldt, T. G.; Montgomery, J. A., Jr. *J. Chem. Phys.* **1991**, *94*, 6091.
(24) Ochterski, J. W.; Petersson, G. A.; Montgomery, J. A., Jr. *J. Chem. Phys.* **1996**, *104*, 2598.
(25) Curtiss, L. A.; Raghavachari, K.; Redfern, P. C.; Stefanov, B. B. *J. Chem. Phys.* **1998**, *108*, 692.
(26) Raghavachari, K.; Stefanov, B. B. Curtiss, L. A. *J. Chem. Phys.* **1997**, *106*, 6764.
(27) Sun, H.; Bozzelli, J. W. *J. Phys. Chem. A* **2001**, *105*, 9543.
(28) Sun, H.; Bozzelli, J. W. *J. Phys. Chem. A* **2003**, *107*, 1018.
(29) Lee, J.; Bozzelli, J. W. *Int. J. Chem. Kinet.* **2003**, *35*, 20.
(30) Sheng, C.; Bozzelli, J. W.; Dean, A. M.; Chang, A. Y. *J. Phys. Chem. A* **2002**, *106*, 7276.
(31) Tsang, W. *Heats of Formation of Organics Free Radicals by Kinetic Methods in Energetics of Organic Free Radicals*; Martinho Simoes, J. A., Greenberg, A., Liebman, J. F., Eds.; Blackie Academic and Professional: London, U.K., 1996.
(32) Melius, C. http://z.ca.sandia.gov/~melius/. Unpublished data.
(33) Knyazev, V. D.; Slagle, I. R. *J. Phys. Chem. A* **1998**, *102*, 1770.
(34) Chen, C.; Bozzelli, J. W. *J. Phys. Chem. A* **2000**, *104*, 4997.
(35) Blanksby, S. J.; Ramond, T. M.; Davico, G. E.; Nimlos, M. R.; Kato, S.; Bierbaum, V. M.; Lineberger, W. C.; Ellison, G. B.; Okumura, M. *J. Am. Chem. Soc.* **2001**, *123*, 9585.
(36) Petersson, G. A.; Al-Laham, M. A. *J. Phys. Chem.* **1991**, *94*, 6081.
(37) Montgomery, J. A., Jr.; Petersson, G. A. *J. Phys. Chem.* **1994**, *101*, 5900.
(38) Ochterski, J. W.; Petersson, G. A.; Wiberg, K. *J. Am. Chem. Soc.* **1995**, *117*, 11299.
(39) Hehre, W. J.; Radom, L.; Schleyer, P. R.; Pople, J. A. *Ab Initio Molecular Orbital Theory*; Wiley: New York, 1986.
(40) Lay, T. H.; Bozzelli, J. W. *J. Phys. Chem.* **1997**, *101*, 9505.
(41) Chen, C.; Bozzelli, J. W. *J. Phys. Chem. A* **2000**, *104*, 9715.
(42) Sun, H.; Bozzelli, J. W. *J. Phys. Chem. A* **2001**, *105*, 4504.
(43) Zhu, L.; Bozzelli, J. W. *J. Phys. Chem. A* **2002**, *106*, 345.
(44) Pitzer, K. S.; Gwinn, W. D. *J. Chem. Phys.* **1942**, *10*, 428.
(45) Petersson, G. A. (Hall-Atwater Laboratories of Chemistry, Wesleyan University, Middletown, CT 06459); Schwartz, M. (Department of Chemistry, University of North Texas, Denton, TX 76203) Personal communication.
(46) Eckart, C. *Phys. Rev.* **1930**, *35*, 1203.
(47) Schwartz, M.; Marshall, P.; Berry, R. J.; Ehlers, C. J.; Petersson, G. A. *J. Phys. Chem. A* **1998**, *102*, 10074.
(48) Troe, J. In *Combustion Chemistry*; Gardiner, W. C., Jr., Ed.; Springer-Verlag: New York, 1984.
(49) Knyazev, V. D. *J. Phys. Chem.* **1996**, *100*, 5318.
(50) Bozzelli, J. W.; Chang, A. Y.; Dean, A. M. *Int. J. Chem. Kinet.* **1997**, *29*, 161.
(51) Dean, A. M.; Bozzelli, J. W. In *Gas-Phase Combustion Chemistry, Chapter 2: Combustion Chemistry of Nitrogen*; Gardiner, W. C., Jr., Ed.; Springer-Verlag: New York, 1999; ISBN 0-387-98861-0.
(52) Stull, D. R.; Westrum, E. F., Jr.; Sinke, G. C. *The Chemical Thermodynamics of Organic Compounds*; Robert E. Krieger Publishing: Malabar, FL, 1987.
(53) Rodgers, A. S. *Selected Values for Properties of Chemical Compounds*; Thermodynamic Research Center, Texas A&M University: College Station, TX, 1982.
(54) Marshall, P. *J. Phys. Chem. A* **1999**, *103*, 4560.
(55) Pedley, J. B.; Naylor, R. O.; Kirby, S. P. *Thermodynamic Data of Organic Compounds*, 2nd ed.; Chapman and Hall: London, U.K., 1986.
(56) Mayer, P. M.; Glukhovtsev, M. N.; Gauld, J. W.; Radom, L. *J. Am. Chem. Soc.* **1997**, *119*, 12889.
(57) Stull, D. R.; Prophet, H. *JANAF Thermochemical Tables*, 2nd ed. (NSRDS-NBS37); U.S. Government Printing Office: Washington, DC, 1970.
(58) Lee, J.; Chen, C.; Bozzelli, J. W. *J. Phys. Chem. A* **2002**, *106*, 7155.
(59) Ervin, K. M.; Deturi, V. F. *J. Phys. Chem. A* **2002**, *106*, 9947.

(60) Ritter, E. R.; Bozzelli, J. W. *Int. J. Chem. Kinet.* **1991**, *23*, 767.
(61) Ritter, E. R. *J. Chem. Inf. Comput. Sci.* **1991**, *31*, 400.
(62) Reid, R. C.; Prausnitz, J. M.; Sherwood, T. K. *The Properties of Gases and Liquids*; McGraw-Hill: New York, 1979.
(63) Kang, J. K.; Musgrave, C. B. *J. Chem. Phys.* **2001**, *115*, 11040.
(64) Zhang, Y. K.; Yang, W. T. *J. Chem. Phys.* **1998**, *109*, 2604.
(65) Johnson, B. G.; Gonzales, C. A.; Gill, P. M. W.; Pople, J. A. *Chem. Phys. Lett.* **1994**, *221*, 100.
(66) Jursic, B. S. *Chem. Phys. Lett.* **1996**, *256*, 603.
(67) Kee, R. J.; Rupley, F. M.; Miller, J. A. *Chemkin-II: A Fortran Chemical Kinetics Package for the Analysis of Gas Phase Chemical Kinetics*; Sandia National Laboratories: Livermore, CA, 1989.
(68) Baulch, D. L.; Cobos, C. J.; Cox, R. A.; Esser, C.; Frank, P.; Just, Th.; Kerr, J. A.; Pilling, M. J.; Troe, J.; Walker, R. W.; Warnatz, J. *J. Phys. Chem. Ref. Data* **1992**, *21*, 411.
(69) Taylor, P. H.; Rahman, M. S.; Arif, M.; Dellinger, B.; Marshall, P. *26th Symposium (International) on Combustion*; The Combustion Institute: Pittsburgh, PA, 1996; p 497.
(70) Maricq, M. M.; Szente, J. J. *J. Phys. Chem.* **1996**, *100*, 12380.
(71) Chen, C.; Bozzelli, J. W. *J. Phys. Chem. A* **1999**, *103*, 9731.
(72) Tsang, W.; Hampson, R. F. *J. Phys. Chem. Ref. Data* **1986**, *15*, 1087.
(73) Ernst, J.; Spindler, K.; Wagner, H. Gg. *Ber. Bunsen-Ges. Phys. Chem.* **1976**, *80*, 645.